Additive effects of nano-filler on mechanical and electrical properties of polymer materials

by

Masato Hamadate

submitted to Kitami Institute of Technology

in partial fulfillment of the requirements for the degree of

Doctor of Philosophy

Supervisor: Professor Dr. Hisayuki Nakatani

Kitami Institute of Technology

March, 2016

Referees-in-chief: Professor: Professor Dr. Masayuki Hoshi

Kitami Institute of Technology

Referees: Professor Dr. Toru Saito

Kitami Institute of Technology

Referees: Associate Professor Dr. Noriyasu Okazaki

Kitami Institute of Technology

Referees: Associate Professor Dr. Hirohumi Arai

Kitami Institute of Technology

Referees: Professor Dr. Hisayuki Nakatani

Nagasaki University

Chapter 1:
General Introduction

Chapter 2:

Interface Adhesion Properties of Syndiotactic Polypropylene/Cellulose Group Composite: Relationship Between Chemical Structure of Coupling Agent and Reactivity for Cellulose Group

Chapter 1

General Introduction

1-1 Plastics materials

In general, polymers are comprised of a series of a repeating unit. Prior to becoming a repeat unit in a polymer chain, these mall monomers include a double bond between two carbon atoms and four pendant groups attached to these two carbons. The term polymerization refers to the process of combining these monomers into very long chains which we know as polymers. Most of the time, this is accomplished using heat and pressure. Polymerization has three stages. First step, the polymer chain is initiated by a catalyst of some sort and the chain begins to grow. The second step is the propagation phase. During this stage, the monomers continue to attach to one another until the final stage occurs. The third stage closes the polymer chain. This usually occurs by two growing chains combining to form one finished polymer chain [1].

1-2-1 Polypropylene

Propylene was first polymerized by Giulio Natta and his coworkers in March 1954 [2]. It is the most important commercial polyolefin. Ziegler-Natta catalysts can make highly isotactic polypropylene. The highly isotactic polypropylene is responsible for its high melting temperature and crystallinity, rigidity, toughness, and heat resistance [3]. Currently, isotactic polypropylene(iPP) is used in various field, such as film, battery cases, container, crates, automotive parts, electrical components, medical are and so on [4].

The world production of PP has grown from around 1.5 million tons in the 1970's to over 70.0 million tons in 2008 [5]. It is expected that the production will exceed 89.8 million tons in 2014. Such drastic growth is due to cost performance, excellent

properties, strong and continuous expansion of process versatility, and environmental friendly processes and materials, during manufacturing, use, and polymer recycling process [6,7].

1-2-2 Syndiotactic PP

It has been known that PP is semi-crystalline that has an effect on morphology. The ability of crystallization of chain is a critical factor governing the morphology. The crystallinity of PP is governed primarily by the stereoregularity of the chain. In general, PP is classified into three types by the arrangement of the methyl group. It is defined meso or receme units. In the chain(Figure 1.2(a)). In the case of syndiotactic PP (sPP), the methyl groups have an alternating configuration with respect to the main chain (Figure 1.2(b)). In the case of atactic PP, the methyl groups have random cofiguration(Figure 1.2(c)).

This stereoregularity affects not only crystal structure and physical properties but also oxidative degradation behavior. iPP is major commodity plastic material. However, it cannot be used without stabilizers because of susceptibility to air oxidation. In the case of industrial applications, serious problems have been raised by various molding processes. In the case of daily use, the product of iPP degrades over a period of week or months depending on the physical form, temperature, sun-light,available oxygen, atmospheric pollutants, and so on [8,9].

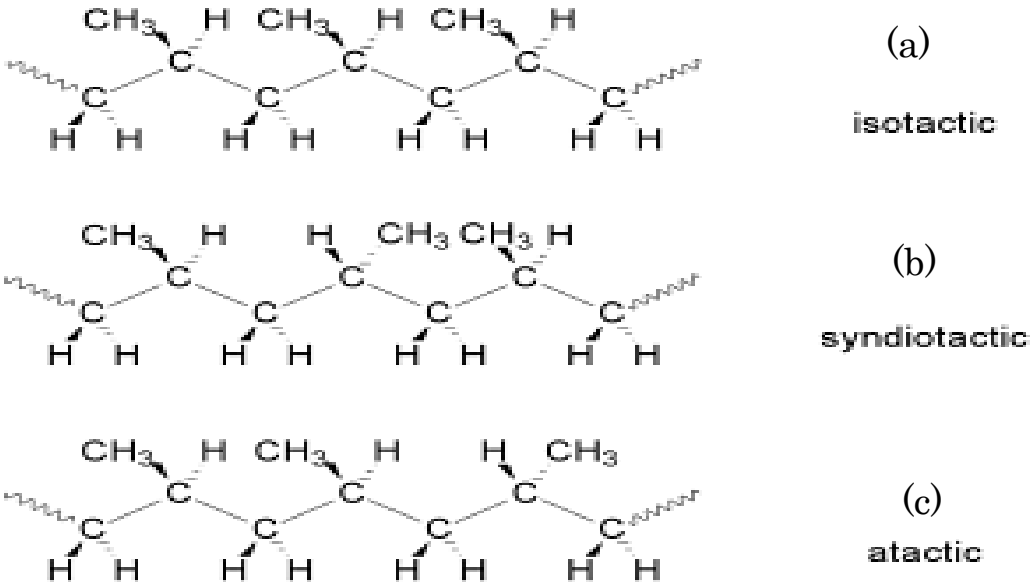

Fig.1 Illustration of the stereo chemical configuration of PP

1-3 Polystyrene

History of styrene and polystyrene from 1839 through 1952 appears in the Styrene monograph edited by Boundy and writer but now out of print. Updating of the story by several teams of Dow writers appeared in the Kirk-Othmer Encyclopedia, the Encyclopedia of Polymer Science and Technology, and the SPE Award address of Amos. We propose a more personalized history written from the perspective of one whose 40-year professional career was involved in scientific and technological aspects of the subject. We view this history as a complex interplay of science, technology, industrial activity, management decisions, legal and patent activities, people, and the vagaries of World War II. Germany had an early industrial lead prior to 1941 with a monomer process and mass polymerization techniques. Original work on styrene-butadiene elastomers was another first. Germany also had a scientific lead as academic scientists

such as Staudinger, Kern, Schulz, Jenckel, and Ueberreiter became involved in the chemistry and physics of styrene and polystyrene [10].

1-4 Polybutene

Polybutene-1 (PB-1) was first synthesized in 1954, one year after polypropylene. It took another 10 years until Chemische Werke HULS, Germany, started the first industrial production in 1964 (capacity: ca. 3 kt/a). Vestolen BT was introduced to the market soon afterward .

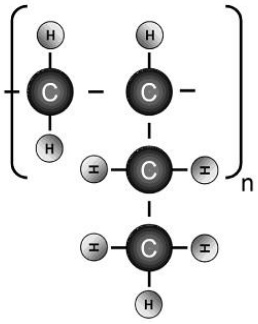

Fig.2 Polybutene-1

Polybutene exists in two isomeric forms depending on where the carbon double bond is positioned in the monomer molecule. If it is between the first and second carbon atoms in a linear molecule (butane-1), then the chemically accurate name of the resulting polymer molecule then the resulting polymer is called polyisobutylene.

The polymer we are concerned with is PB-1. IN the past this polymer has been referred to as polybutylene. PB, PB-1 and polybutene, as well as its chemically correct name, PB-1. PB-1 is obtained by polymerization of butane-1 with a stereospecific Z-N catalyst to create a linear, high molecular, isotactic, semi-crystalline polymer. PB-1 combines the typical properties of conventional polyolefins with some characteristics of technical polymers. In chemical structure PB-1 differs from polyethylene and polypropylene only by the number of carbon atoms in the monomer molecule [11].

1-5 Cellulose

Cellulose is the most abundant and widely used polymer in the world. As the major constituent of plant matter, billion of tons of it are created each year through photosynthesis. In the form of wood, paper, cotton textiles, rayon, film, coatings, and a myriad of other uses including fuel, we consume about 450,000,000 tons of cellulose per year [12].

The cellulose is polysaccharides only consisting of glucose which is made from carbon, hydrogen, oxygen, and glucose is produced by the photosynthesis of the plant. In cell wall of the plant, hemicellulose, lignin and cellulose exist. Therefore, relative content rate of cellulose is 40-70% in the plant.

The advantage of cellulose is low cost, low density, renewability, biodegradability, nontoxicity. The cellulose also has attracted much attention of many researchers as composite materials [13-25]. In particular, the attention has recently concentrated on its biodegradability and renewability from the viewpoint of environmental advantage. Composite based o cellulose has been considered a useful way to employ such features.

1-6-1 Carbon nanotube

Carbon nanotubes (CNTs) are the hottest topic physics, according to a 2006 ranking of different scientific fields in the published literature. The interest in these objects has been sparked by the exceptional properties of those nano-sized objects combined with the ease of theoretical investigations due to the relatively limited number of atoms in CNTs, facilitating *ab initio* calculations. CNT properties reveal many interesting features which are very attractive for solving the technological hurdles that the

semiconductor industry is facing if scaling of circuits continues for another decade. The high current carrying capacity, high thermal conductivity and reduced charge carrier scattering combined with the huge resilience of CNTs promise to solve challengers in the interconnect area, whereas the low effective electron and hole mass, the attractive band gap and the absence of dangling bonds address the need of a fast, energy efficient and high-k dielectric-compatible device of the future [26].

1-6-2 Multiwall Nanotubes

Multiwall carbon nanotubes is a little bit more complex, since it involves the various ways graphenes can be displayed and mutually arranged within filamentary morphology. A similar versatility can be expected to the usual textural versatility of polyaromatic solids. Their diffraction patterns are difficult to differentiate from those of anisotropic polyaromatic solids. The easiest MWNT to imagine is the concentric type (c-MWNT), in which SWNTs with regularly increasing diameters are coaxially arranged into a multiwall nanotube. Such nanotubes are generally formed either by the electric arc technique (without the need for a catalyst), by catalyst-enhanced thermal cracking of gaseous hydrocarbons, or by CO disproportionation [27].

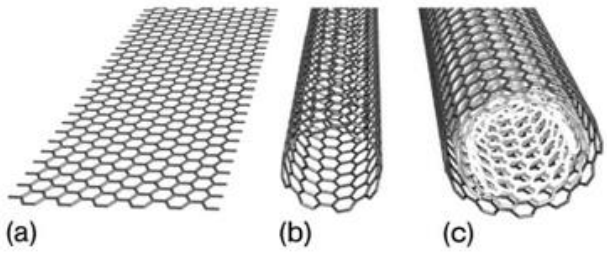

Fig.3 (a) Structure of a single layer of graphite (graphene) (b) single-walled carbon nanotube (c) multi-walled carbon nanotube with tree shells [28]

1-7 Compatibiliser

Attention has been paid to improving the compatibility of the filler with the polymer matrix, by providing an interaction between the filler and the polymer, There are several types of “Compatibilisers”. First type, it can be chemically attached either to a filler (e.g.cellulose fibers), or to a polymer. Second type, it can form a covalent chemical bond between filler and polymer. Third type, it can help to form a sort of uniform “alloy” between two or several polymeric components ordinarily not very compatible with each other. Generally, compatibilizers can improve adhesion between fiber and plastic and markedly improve physical properties of the polymeric composite, its weatherability, and overall performance [29].

1-8-1 Electronically conductive polymer

The ability of polymers to act as electrical insulators is the basis for their widespread use in the electrical and electronic fields, the resistivity of which is generally around $10^{15}\Omega$m. However, material designers have sought to impart conduction to polymers by blending insulating polymers with conductive ingredients such as carbon blacks, carbon fibers, metal particles or conducting polymers such as polyaniline [30]. As a consequence, a range of so-called conductive polymer composite has come to existence since the 1950s [31] with the resistivity between metallic conductor (10^{-7} Ω m) and insulating materials (10^{15} Ω m) [32], which can find their applications in many fields such as floor heating elements, electronic equipment [33, 34], important strategic materials such as electromagnetic interference (EMI) shielding [35], apart from the

conventional application of semi-conducting materials for dissipation of static electricity [36]. More recently conductive composites have been used for sensing components [37, 38]. Compared with metallic conductor, conductive polymer composites have the advantages of ease of shaping, low density, and wide range of electrical conductivities as well as corrosion resistance [39]. Nowadays, carbon black particles and carbon fibers are the most commonly used conductive components to incorporate conduction to polymer composite. The reason for this is that carbon black particles have a much greater tendency to form a conductive network due to their chainlike aggregate structures compared with other conducting additives such as metal powder. Whilst carbon fibers may be considered as chain-like aggregates of carbon particles having long chain length [40].

1-8-2 Percolation

Many conductive polymer composites exhibit percolation characteristic [41]. The curve of conductivity versus filler concentration is S-shaped, which clearly demonstrates a relative narrow filler loading range during which a small increase in loading will result in a drastic increase in conductivity. This change implies some sudden changes in the dispersing state of conductive particles, i.e. the coagulation of particles to form networks which facilitates the electrical conduction through the composites. Put in another way, the composite exhibits an insulator to conductor transition. The critical amount of filler necessary to build up a continuous conductive network and accordingly to make the material conductive is referred to as the percolation threshold. A critical aspect in the production of conductive polymer composites is the filler content, which

must be as low as possible and still allows the composite to fulfill its electrical requirements, otherwise the mixture processing becomes difficult, the mechanical properties of the composite are poor and the final cost is high. There are several ways to decrease the percolation threshold of conductive filler concentration in polymeric matrices, which are mainly based on the use of additives, the optimization of processing conditions, as well as the size, distribution and porosity of filler [42].

References

1. M. Kutz, *Applied Plastics Engineering Handbook: Processing and Materials.* USA. 2011.
2. P. J. T. Morris, *Polymer Pioneers,* 2005.
3. J. P. Soares, L. C. Simon, T. Meyer and T. F. Keurentijes Eds., WILEY-VCH Verlag Gmbh & Co. KCaA, Germany, Weinheim, 2005.
4. T. Meyer and, T. F. Keurentijes, T. Meyer and, T. F. Keurentijes Eds., *Handbook of polymer Reaction Engineering*., WILEY-VCH Verlag GmbH & Co. KCaA, Weinheim, 2005.
5. "Future supply and demand trend of world petrochemical products", *Report of Ministry of Economy, Trade and Industry of Japan*, 2010.
6. N. P. Cheremisinoff, *Guidbook to commercial polymers, properties and applications*, PTR Prentice Hall, New Jersey, 1993.
7. R. B. Saymour, C. Vasile, M. rusu, *Handbook of polyolrefins*, Marcel Dekker, New York, 1993.
8. R. F. Becker, L. P. J. Burton, S. E. Amos, E. P. Moore Jr. Eds., *Polypropylene Handbook*, Carl Hanser Verlag, New York, 1996.
9. T. Q. Nguyen, T. Meyer and T. F. Keurentjes Eds., *Handbook of Polymer Reaction Engineering*, WILEY-VCH Verlag GmbH & Co. KCaA, Germany, Weinheim, 2005.
10. R. F. Boyer, "Anecdotal History of Styrene and Polystyrene." *J. Macromol. Sci. —Chem.* 1981, 33-41.
11. M. Kutz, *Applied Plastics Engineering Handbook: Processing and Materils.* USA. 2011.

12. E. Ott, H. M. Spurlin, Eds., *Cellulose and Cellulose Derivatives,* Interscience Pubilisyers, New York, **1954**.

13. S. Takase, N. Shraishi, *J.Appl. Polym. Sci.*, **1989**, 37, 645.

14. D. Maldas, B. V. Kokta, C. Daneault, *J. Appl. Polym. Sci.*, **1989**, 37, 751.

15. R. G. Raj, B. V. Kokta, D.Maldas, C. Daneault, *J. Appl. Polym. Sci.*, **1989**, 37, 1089.

16. P. Hedenberg, P. Gatenholm, *J. Appl. Polym. Sci.*, **1996**, 60, 2377.

17. F. Zhang, W. Qiu, L. Yang, T. Endo, *J. Mater. Chem.*, **2002**, 12, 24.

18. W. Qiu, F. Zhang, T. Endo, T. Hirotsu, *J. Appl Polym. Sci.*, **2003**, 87 337.

19. W. Qiu, F. Zhang, T. Endo, T. Hirotsu, *J. Appl Polym. Sci.*, **2004**, 91 1703.

20. J. M. Felix, P. Gatenholm, *J. Appl. Polysm. Sci.*, **1991**, 42, 609.

21. W. Qiu, F. Zhang, T.Endo, T. Hirotus, *J. Appl. Polym. Sci.*, **2004**, 94, 1326.

22. V. N. Hristov, S. T. Vasileva, M. Krumova, R. Lach, G. H. Michler, *Polym. Compos*, **2004**, 25, 521.

23. D. Nwabunma, T. Kyu, *Polyolefin composites*, John Wiley and Sons. Hodoken, New Jersey, **2008**, 33.

24. B. Oliver, K. F. Gary, H. Christofer, G. K. Jan, O. Tabata, WILEY-VCH Verlag GmbH & Co. *Carbon Nanotube Devices: Properties, modeling, Integration and Applications,* **2008**, 1-2.

25. B. Bhushan,. Springer-Verlag. *Springer handbook of Nanotechnology.* Berlin, **2010**.

26. B. Oliver, K. F. Gary, H. Christofer, G. K. Jan, O. Tabata,. WILEY-VCH Verlag GmbH & Co. *Carbon Nanotube Devices: Properties, modeling, Integration and Applications,* **2008**.

27. A. A. Klyosov, *Wood-Plastic Composetes*, John Wiley ans Sons. Hodoken, New Jersey, **2007**.

28. M. Narkis, M. Zilberman, A. Siegmann, *Polym. Adv. Technol.* **1997**, 8, 525.

29. E. Frydman, UK Patent **1948**, 604695, 8.

30. R. M. Scarisbrick, *J. Phys.* D: *Appl Phys.* **1973**, 6, 2098.

31. A. Y. Xiao, Q. K. Tong, A. C. Savoca, O. H. Van, Trans Compon Pack Technol. **2001**, 24, 445.

32. T. Fujitani, K. Matsuoka, US4258100, Mar. 24, **1981**.

33. S. K. De, J. R. White, *Short fibre-polymer composites*. Woodhead Publishing Limited, Cambridge England, **1996**, p 182.

34. R. H. Norman, *Conductive rubbers and plastics*. Elsevier Publishing Company Limited, Amsterdam, **1970**, p 224.

35. L. Flandin, Y. Brechet, J. Y. Cavaille, *Compos. Sci. Technol.*, **2001,** 61, 895.

36. X. Wang, D. D. L. Chung, Sensor Actuator A, **1998,** 71, 208.

37. R. H. Norman, *Conductive rubbers and plastics*. Elsevier Publishing Company Limited, Amsterdam, **1970**, p 3.

38. W. Zhang, A. Abbas, S. Dehghani, S. B. Richard, *J. Mater. Sci.* **2007,** 42, 3408-3418.

39. V. Y. Gul, N. S. Maizel, A. N. Kamenskii, N. M. Fodiman, S. Vysokomol, Transl. *Polymer Sci.* USSR, **1962**, 4, 642.

40. K. T. Chung, A. Sabo, A. P. Pica, *J. Appl. Phys,* **1982,** 53, 6867.

41. G, T, Mohanraj, T. K. Chaki, A. Chakraborty, D. Khastgir, *J. Appl. Polym. Sci.* **2004**, 92, 2179.

42. J. H. Smuckler, P. M. Finnerty, *Adv. Chem. Ser.* **1974**, 134, 171.

Chapter 2

Interface Adhesion Properties of Syndiotactic Polypropylene/Cellulose Group Composite: Relationship Between Chemical Structure of Coupling Agent and Reactivity for Cellulose Group

2-1: Introduction

Cellulose has been one of the most popular polymeric materials in the world and has been used as raw materials of building materials and paper for a long time ago. Cellulose is low cost, high modulus, renewable, and biodegradable material. Recently cellulose has attracted much attention as composite material[1–10] since it has great potential for the preparation of composite materials having high modulus and renewability. As most popular composite based on cellulose, the composite with polyolefin such as isotactic polypropylene (IPP) has been extensively prepared. However, FC is hydrophilic and tends to aggregate, causing poor processability and inherent incompatibility with hydrophobic polyolefin. The improvements of these properties have been studied on the modifications of FC surface. Silane coupling agent is one of the adhesion promoter and is often employed in the FC composite.[11] Adequate silanization brings about a higher FC dispersion in the polyolefin matrix and an interface having a good adhesion strength. In our previous work,[12] the silanized FC with APTMS showed a good adhesion strength to syndiotactic PP(SPP) matrix. The APTMS silanization brought about an excellent improvement of SPP/FC tensile properties such as the

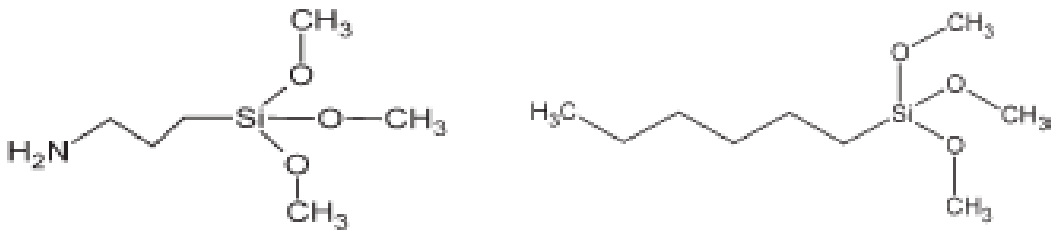

Fig.1 Chemical structures of APTMS and HTMS.

Young's modulus, and the improvement degree increased with the increase of the APTMS content in the silanization.

The APTMS has two kinds of bifunctional group. As shown in Figure 1, one is methoxyl

group and the other is amino one. The amino group has an ability to catalyze the reaction between silane molecules and silanol groups to form siloxane bond.[13,14] Therefore, aminoalkoxysilane is easily polymerized.[14] In addition, amino group has an ability to form hydrogen bonding with ROH[15] or SiOH[14] groups. These amino group functionalities are believed to contribute to the excellent improvement of SPP/FC tensile properties. The purpose of the present work is to clarify the effects of the APTMS silane coupling agent on the FC modification. The APTMS silanization certainly affects physical properties of the FC itself, leading to the improvement of the SPP/FC composite. To clarify the APTMS role, the FC silanization with hexyltrimethoxysilane (HTMS) having nonpolar hexyl group has been performed, and the morphology and the tensile properties of the SPP/silanized FC with the HTMS have been studied as compared with those of the SPP/silanized FC with the APTMS. The ATMS permeates the FC and would affect the hydrogen bonding among celluloses in it. The polarity difference between the APTMS and the HTMS would reveal a change of the hydrogen bonding among celluloses in the silanized FC. In addition, an additive effect of high molecular weight SPP-g-DMI on the morphology and the tensile properties of the SPP/FC also have been studied. The SPP-g-DMI is unable to penetrate into the FC because of its high molecular weight, and the reaction with the OH group in cellulose is confined on the FC surface. The differences between the APTMS silanization and the SPP-g-DMI would reveal the change of the FC itself by the silanization. Moreover, the SPP/silanized HC with the APTMS have prepared, and the morphology and the tensile properties have been also studied as compared with those obtained from the SPP/HC with the SPP-g-DMI additive agent.

2-2 Experimental

2-2-1 Materials

SPP was supplied by Sanwayuka Industry Co. The trade name is TOTAL 1751. The number-average molecular weight (M_n) and the polydispersity (M_w/M_n) were 3.5×10^4 and 3.0, respectively. FC (W- 100GK) was donated by Nippon Paper Chemicals Co. Ltd. The FC was dried in desiccator for 7 days before preparation. The moisture of the FC was below 0.7 wt %. The FC dimensions are over 90 wt % pass 100 mesh (below 150 μm), the average length was ~ 37μm; 3-aminopropyltrimethoxysilane (APTMS) and hexyltrimethoxysilane (HTMS) were purchased from Shinetsu Silicon Chemicals Co. The chemical structures of APTMS and HTMS are shown in Figure 1. Methanol and dimethyl itaconate (DMI) were purchased from Wako Pure Chemical Industry, respectively. Dicumyl peroxide (DCP) was purchased from Sigma Aldrich. These were used without further purification.

2-2-2 Preparation of holocellulose (HC)

A dwarf bamboo (*Sasa kurilensis*) was treated by chlorite to remove lignin component,[16] was enough dried in desiccator and then was ground by a vibration mill pot. The average length of the sample was ~ 75μm. The sample was used as "HC."

2-2-3 Silanization

Mixing of 30 mL methanol solution of the silane coupling agent (APTMS or HTMS) and the FC (1 g) were performed using a 0.1-L glass equipped with a stirrer at 23℃ for 24 h. The methanol solvent was evaporated using a rotary evaporator. The samples obtained

were dried at 60℃ for 6h at in a vacuum oven and were used as “silanized FC or HC.”

2-2-4 Synthesis of SPP grafted with dimethyl itaconate (SPP-g-DMI)

The SPP was reprecipitated from a boiling xylene solution into methanol and dried at 60℃ for 8 h and was used as the sample without antioxidant. The synthesis of SPP-g-DMI was carried out with an Imoto Seisakusyo IMC-1884 melting mixer. The SPP (2 g), DMI (0.2 g), and DCP radical initiator (0.016 g) were sequentially added, and their mixing was performed at 180℃

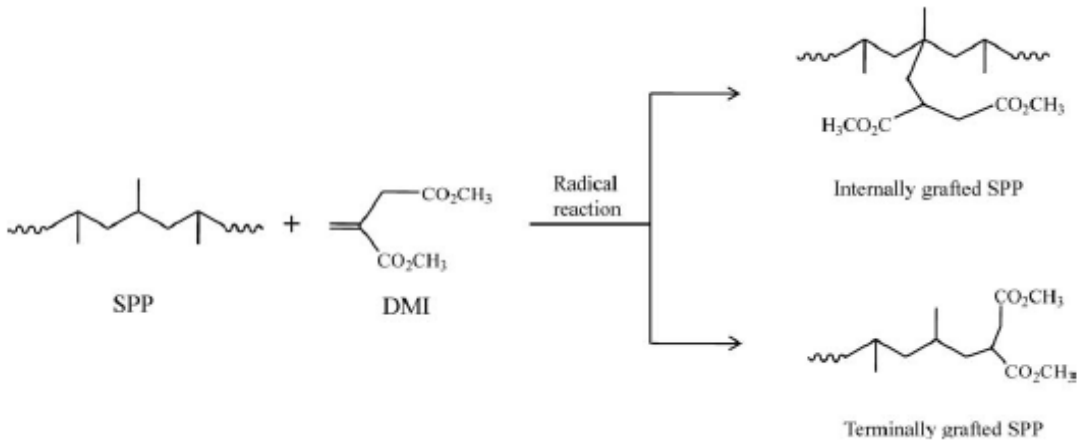

Fig.2 Chemical structure model of SPP-g-DMI.

at 100 rpm for 60 min. The sample obtained was first dissolved in xylene at its refluxing temperature under nitrogen atmosphere, and the solution was precipitated by pouring into methanol. The precipitate obtained was washed repeatedly with fresh methanol, was dried in a vacuum oven at 60℃ for 7 h and was used as the SPP-g-DMI sample. The M_n and M_w/M_n were 3.3×10^4 and 2.3, respectively. The chemical structure[17] is shown in Figure 2. The grafting rate was measured by FTIR spectroscopy [17] and was 0.11 wt %.

2-2-5 X-ray photoelectron spectroscopy (XPS) measurement

In the case XPS measurement, the silanized FC and HC were purified by a Soxhlet-extraction with boiling acetone for 8 h to remove the silane, which was not chemically bonded to the FC and HC surfaces. The X-ray photoelectron spectra of the silanized samples were measured by an X-ray Photoelectron Spectrometer (Rigaku XPS-7000) with an unmonochromated magnesium Ka source (1253.6 eV). The magnesium K_α source was operated at 10 kV and 5 mA or at 10 kV and 30 mA. The samples were mounted onto a holder with double-sided adhesive tape and placed in a vacuum in the range 1.33×10^{-6} to 1.33×10^{-5} Pa. The analyzed sample area was ~ 4 mm × 6 mm. The atomic percentages of the elements present were derived from spectra run of the corresponding region.

2-2-6 Preparation of composites

Composites are prepared by an Imoto Seisakusyo IMC-1884 melting mixer. All mixtures were carried by each weight ratio. After a small amount of phenolic antioxidant (Adekastab AO-60, ~ 0.5%) was added, the mixing was performed at 150℃ at 60 rpm for 5 min. The composites obtained were molded into the film (100 μm) by compression molding at 150℃ under 4 MPa for 5 min.

2-2-7 Scanning electron microscope (SEM) observation

SEM observation was carried out with a JEOL JSM- 5800 at 20 kV. The sample was fractured in liquid nitrogen, and then was sputter-coated with gold.

2-2-8 Tensile testing

Stress-strain behavior was observed using a SHIMADZU EZ-S at a cross-head speed of 3 mm/min. The sample specimens were cut with dimensions 30 × 5 × 0.1 mm shape in which the gauge length was 10 mm. We chose the specialized specimen (like ISO reed-shape) to adapt to the size of our tensile testing machine. All of tensile testing was performed at 20℃. The values of Young's modulus were obtained from the slope of the stress-strain curve (until about 1% of the strain value). All results obtained were the average values of ten measurements.

2-3 Results and discussion

Figure 3 shows the SEM micrographs of fractured surfaces of the SPP/FC and the SPP/silanized FC with the APTMS, with the HTMS and the SPP/SPPg- DMI/FC, respectively. As shown in Figure 3(a), large voids exist between the FC and the SPP matrix, suggesting that the interfacial adhesion is very poor. Whereas, the size of the voids dramatically decreases by the two kinds of silanization and by the addition of the SPP-g-DMI graft-polymer, indicating that the interfacial adhesion is certainly improved. It seems, however, that there are some differences in the morphology of the interface. In

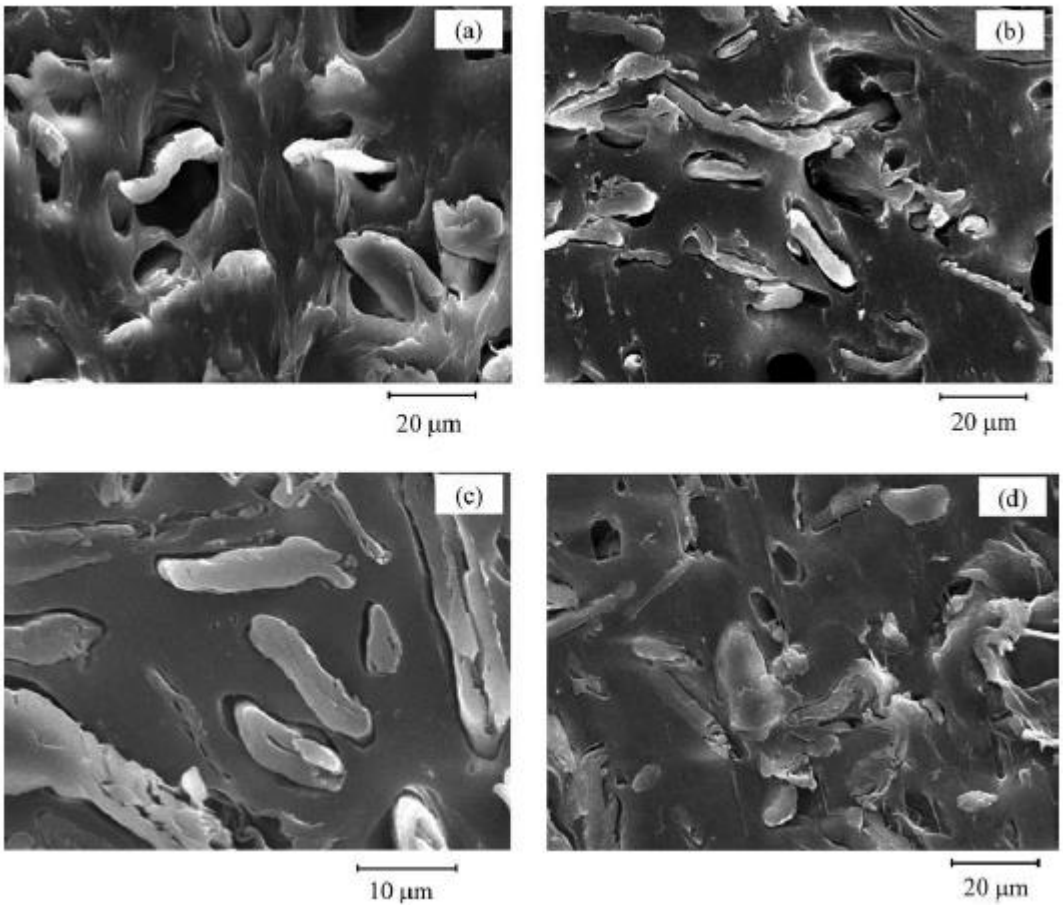

Fig.3 SEM microphotographs of the surfaces of the SPP/FC, of the SPP/silanized FC with APTMS or with HTMS, and of the SPP/SPP-g-DMI/FC. (a): SPP (70 wt %)/FC(30 wt %). (b): SPP (70 wt %)/silanized FC (30 wt %) with APTMS (2 wt %). (c): SPP (70 wt %)/silanized FC (30 wt %) with HTMS (2 wt %). (d): SPP (60 wt %)/SPP-g-DMI (10 wt %)/FC (30 wt %).

the case of the SPP/silanized FC with the HTMS, it seems that the boundary between the FC and the matrix is much distinct than others. In addition, as shown in Figure 3(c), the cracked FCs can be observed, suggesting that the HTMS silanization brings about an embrittlement of the FC.

Figure 4 shows the changes of the Young's moduli of the SPP(70%)/silanized FC(30%) composites with various contents of the APTMS, the HTMS and of the SPP ((70 - x) wt %)/SPP-g-DMI(x wt %)/FC (30 wt %) composite, respectively. In the cases of the SPP/silanized FC with the APTMS and the SPP/ SPP-g-DMI/FC, the Young's moduli

linearly increase with the increases of these agent contents, suggesting that the adhesive strengths of these interfaces are reinforced by the APTMS and by the SPP-g-DMI, respectively. Whereas, in the case of the SPP/silanized FC with the HTMS, the Young's moduli reach the maximum at the 1 wt % HTMS content and then decrease with the HTMS content.

Figures 5 and 6 show the changes of the tensile strengths and the elongations at break of the SPP (70%)/silanized FC (30%) composites with various contents of the APTMS, the HTMS and of the SPP ((70 - x) wt %)/SPP-g-DMI (x wt %)/FC (30 wt %), respectively. In the case of the composite with the APTMS, the tensile strength reaches the maximum value at the 4 wt % APTMS content, and the elongation at break drops rapidly at the 5 wt % content. The embrittlement behavior is explainable in terms of the increase of the interface strength.[7] At the 5 wt %, the interface strength is believed to exceed the native strength of the FC itself. Therefore, the break of the FC occurs under the tensile loading, leading to the crack initiation.[18] In the case of the SPP ((70 - x) wt %)/SPP-g-DMI (x wt %)/FC (30 wt %), the tensile strength linearly increases with the

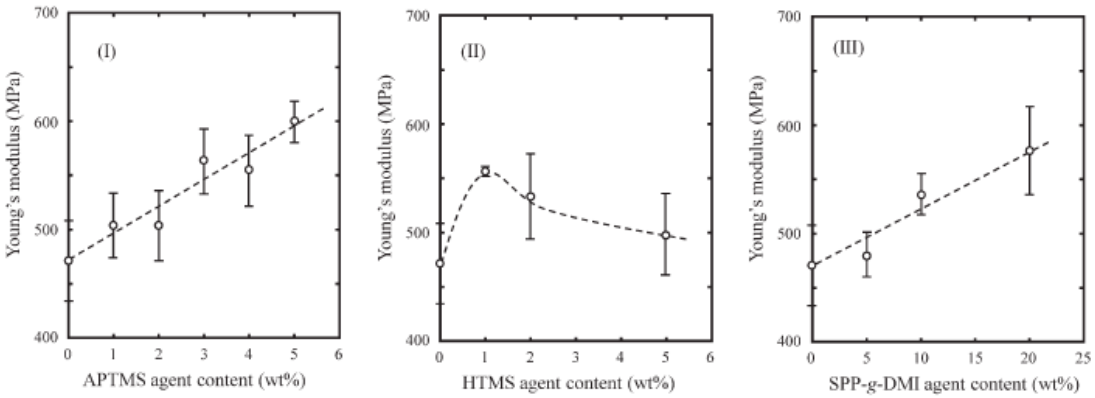

Fig.4 Young's moduli of the SPP/silanized FC with APTMS or with HTMS, and of the SPP/SPP-g-DMI/FC (I): SPP (70 wt %)/silanized FC (30 wt %) with various content of APTMS. (II): SPP (70 wt %)/silanized FC (30 wt %) with various content of HTMS. (III): SPP ((70 _ x) wt %)/SPP-g-DMI (x wt %)/FC (30 wt %).

increase of the SPP-g-DMI amount, and the elongation at break linearly decreases with the increase of the one.

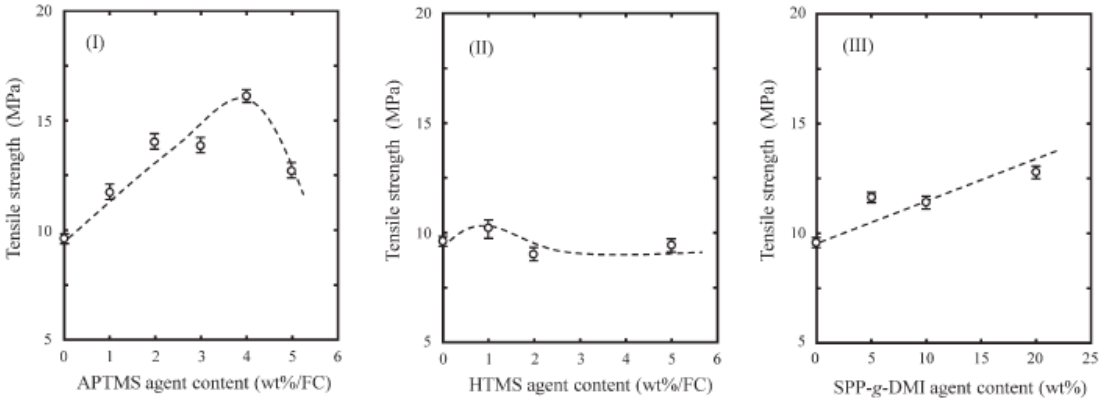

Fig.5 Tensile strengths of the SPP/silanized FC with APTMS or with HTMS, and of the SPP/SPP-g-DMI/FC (I): SPP (70 wt %)/silanized FC (30 wt %) with various content (wt %) of APTMS. (II): SPP (70 wt %)/silanized FC (30 wt %) with various content (wt %) of HTMS. (III): SPP ((70 - x) wt %)/SPP-g-DMI (x wt %)/FC (30 wt %).

The ester groups of the SPP-g-DMI can react with OH groups on the FC. The reaction is a kind of esterification reaction and produces the ester binding between them. The reactivity certainly depends on the SPP-g-DMI amount. The FC is gradually linked to the SPP-g-DMI with the increase of the additive amount, and the interface strength becomes stronger. Since the SPP-g-DMI has the high molecular weight, the degree of the entanglement between the SPP-g- DMI and the SPP chains must be considerably high. Therefore, the entanglement strength is believed to be higher than the FC strength itself. When a stress is applied to the composite, the FC must be preferentially fractured. In Figure 6(III), the embrittlement of the composite is likely due to the increase of the FC destructive deformation, by which formation of void in the SPP matrix is simultaneously caused.[19] Whereas, in the case of SPP (70%)/silanized FC (30%) composites with various content of HTMS, the behavior of the tensile strength and the elongation at break as well as that of the Young's modulus is considerably

strange. The tensile strengths reach the maximum at the 1 wt % HTMS content and then become constant with the higher content. The elongations at break reach the

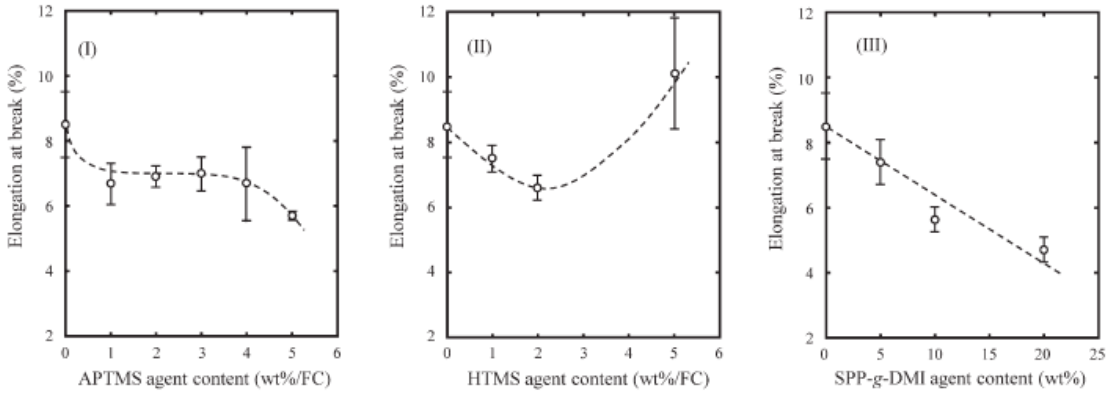

Fig.6 Elongations at break of the SPP/silanized FC with APTMS or with HTMS, and of the SPP/SPP-g-DMI/FC (I): SPP (70 wt %)/silanized FC (30 wt %) with various content (wt %) of APTMS. (II): SPP (70 wt %)/silanized FC (30 wt %) with various content (wt %) of HTMS. (III): SPP ((70 - x) wt %)/SPP-g-DMI (x wt %)/FC (30 wt %).

minimum at the 2 wt % HTMS content and then increase at the 5 wt %. The tensile behavior is considerably different as compared with other samples and would be due to the silanization with the HTMS. The FC is composed of cellulose aggregations. The cohesion force is originated from hydrogen bonding network among the celluloses. As shown in Figure 1, the HTMS has the nonpolar hexyl group in the chemical structure. The hexyl group is located at the one side chain end and converts the cellulose surface into hydrophobicity after the silanization.

The HTMS silanization certainly disturbs the hydrogen bonding network among the celluloses. Therefore, the cohesion force among celluloses becomes weaker with the

TABLE I
Elemental Compositions (mol %) of the FC and the Silanized FC Determined from XPS

			Elemental composition (mol %)				Binding energy (eV)			
Silanized FC	O/C	Si/O	O	C	Si	N	O	C	Si	N
FC	0.85	0.02	45.6	53.5	0.9	0.0	532.9	286.6	101.1	–
Silanization at 2 wt %										
APTMS	0.40	0.40	23.9	59.6	9.5	7.0	532.4	285.0	102.4	398.9
HTMS	0.76	0.05	42.2	55.7	2.1	0.0	533.1	286.8	102.3	–
Silanization at 5 wt %										
APTMS	0.43	0.42	25.0	57.5	10.5	7.0	532.8	285.6	102.8	399.3
HTMS	0.71	0.06	40.4	57.1	2.5	0.0	533.2	286.8	102.4	–

increase of the degree of the silanization, and the silanized FC must be embrittled. In fact, as mentioned above, the cracked FCs can be observed in Figure 3(c). The strange tensile behavior is due to the block of the inter hydrogen bonding formation by the HTMS silanization. When the tensile stress is applied, the weaker FC is preferentially deformed. Many cracks are preferentially generated in the FC, leading to the relaxation of strain constraint.[20] That is, the constant value of the tensile strength and the increase of the elongations at break at the higher HTMS content are due to the FC embrittlement. In addition, it seems that the SPP-g-DMI is unable to penetrate into the FC because of its higher molecules. Therefore, such tensile behavior would be not exhibited in the SPP/ SPP-g-DMI/FC composite series. The elemental compositions obtained from the XPS spectra of the FC and the silanized FCs with the APTMS and the HTMS coupling agents are summarized in Table I. The FC has the oxygen-to-carbon (O/C) atomic ratio of 0.85, and its rate means that the FC is composed of pure cellulose.[15,18] In the cases of the 2 wt % solutions, the O/C ratios for the silanized FCs with the APTMS and the HTMS are 0.40 and 0.76, respectively. The difference suggests that there exists a relationship between the chemical structure of silane coupling agent and the reactivity with the cellulose in the FC. These O/C ratios slightly change against the higher silane coupling agent concentration (5 wt %). In addition, the silanizations with the 5 wt % solution of the silane agents bring about the slight (~ 10%) increases of

TABLE II
Analyses of High Resolution C_{1s} Peaks of the FC, HC, and the Silanized HC with APTMS

	Analysis of C1s peaks (%)			Binding energy (eV)		
Silanized samples	C1	C2	C3	C1	C2	C3
FC	24.5	55.9	19.6	285.0	286.6	288.0
HC	32.0	53.2	14.9	285.0	286.8	288.6
Silanization						
At 1 wt %	32.8	49.9	17.3	284.9	286.7	288.5
At 10 wt %	38.7	46.1	15.2	285.0	286.5	288.3

the Si contents as compared with those with the 2 wt % solution. These silanizations with the higher concentration solution certainly raise the coverage on the cellulose. It is noted here that the Si content in the silanized FC with the APTMS is several times higher than that with the HTMS. The APTMS has the bifunctional nature[13,14] and is likely captured by OH groups on the cellulose because of a hydrogen bonding formation between the cellulose and the APTMS. The covalent bond (-Si-O-C-) formation between them proceeds through the condensation of the hydrogen bonded APTMS. The APTMS shows a higher reactivity against OH group on the cellulose since the amino group exists in the chemical structure. In addition, since the APTMS has the bifunctional nature, the hydrogen bonding between the silanized and the unsilanized celluloses would be kept. Therefore, unlike the HTMS, the APTMS silanization does not bring about the FC embrittlement. The reactivity between silane agent and OH group on the cellulose and the keeping of the hydrogen bonding between the silanized and the unsilanized celluloses are certainly important for reinforcement of tensile properties in SPP/cellulose composite. It is noted here that the FC is composed of only pure cellulose. Practically cellulose materials such as wood flour are composed of not pure cellulose only but various impurities as well. Natural cellulose exists as a mixture of cellulose and hemicellulose. The mixture is called as holocellulose (HC). Since hemicellulose is

TABLE III
Elemental Compositions (mol %) of the HC and the Silanized HC with APTMS

			Elemental composition (mol %)				Binding energy (eV)			
Silanized FC	O/C	Si/O	O	C	Si	N	O	C	Si	N
HC	0.69	0.04	39.8	58.1	1.7	0.4	533.0	286.6	102.1	399.9
Silanization										
At 1 wt %	0.65	0.04	38.5	59.3	1.5	0.7	533.0	286.7	102.4	399.8
At 10 wt %	0.71	0.03	40.7	57.4	1.1	0.8	532.7	286.3	102.1	399.6

Determined by XPS.

composed of a group of complex carbohydrates, the reactivity between the silane agents and the OH groups on the HC must be considerably different from that on the FC (pure cellulose). To study the reactivity with HC, the SPP (70%)/silanized HC (30%) composites with various contents of the APTMS have been prepared and, the tensile behavior and the morphology have been studied. In addition, the tensile behavior and the morphology of the SPP ((70 - x) wt %)/SPP-g-DMI (x wt %)/HC (30 wt %) also have been studied to clarify the reactivity between the HC and the SPPg- DMI.

The analyses of high resolution C_{1s} peaks of the FC, HC, and the silanized HC with APTMS are summarized in Table II. In the case of the C_{1s} spectrum of the FC, it consists of three peaks at ~ 285, 287, and 288 eV, arising from C1 (carbon atoms to a carbon and/or hydrogen atoms (C-C/C-H)), C2 (carbon atoms bonded to a single oxygen atom, other than a carbonyl oxygen (C-OH)), and C3 (carbon atoms bonded to two noncarbonyl oxygen atoms or to a single carbonyl oxygen atom (O-C-O, C=O), respectively.[15] Since the C2 (corresponding to OH group) ratio of the HC is almost the same as that of the FC, the amount of the OH group in the HC must be close to that in the FC. However, in the case of holocellulose obtained from bamboo species such as the Sasa kurilensis, the holocellulose is commonly composed of ~ 70% cellulose and ~ 30% hemicellulose, [21,22] of which major component is xylan. As shown in Figure 7, unlike cellulose, xylan has no primary alcohol having a higher reactivity. If the HC has the same amount of the OH group as the FC, the reactivity with

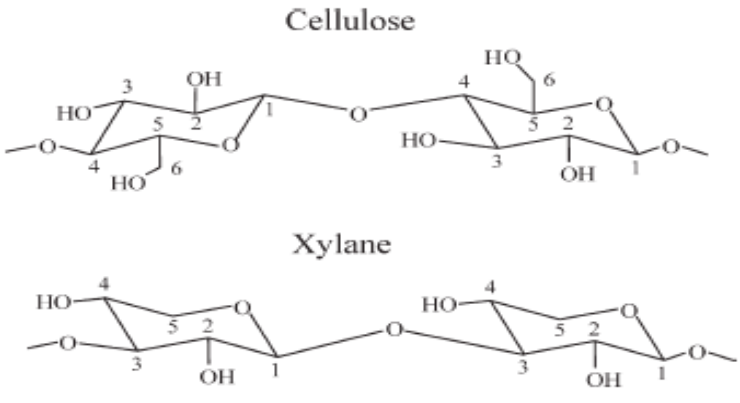

Fig.7 Chemical structures of cellulose and xylane..

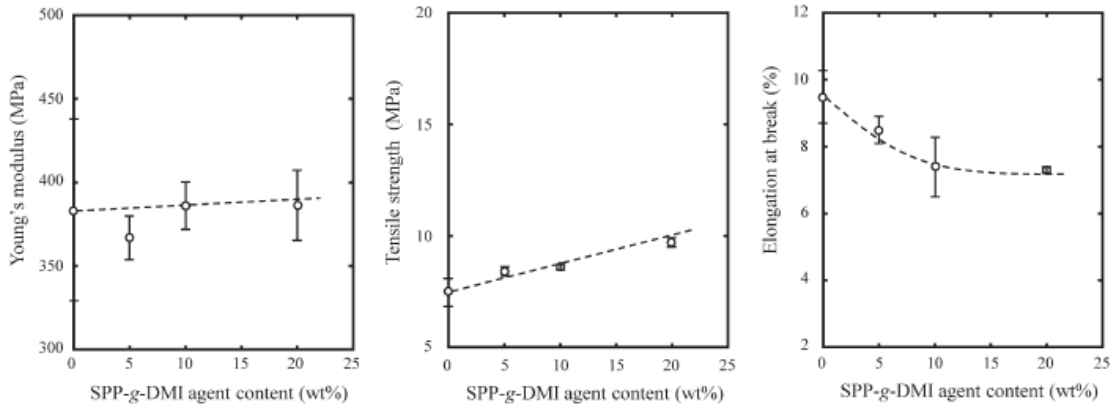

Fig.8 Young's moduli, tensile strengths, and elongations at break of the SPP (70 wt %)/silanized HC (30 wt %) with various content of APTMS.

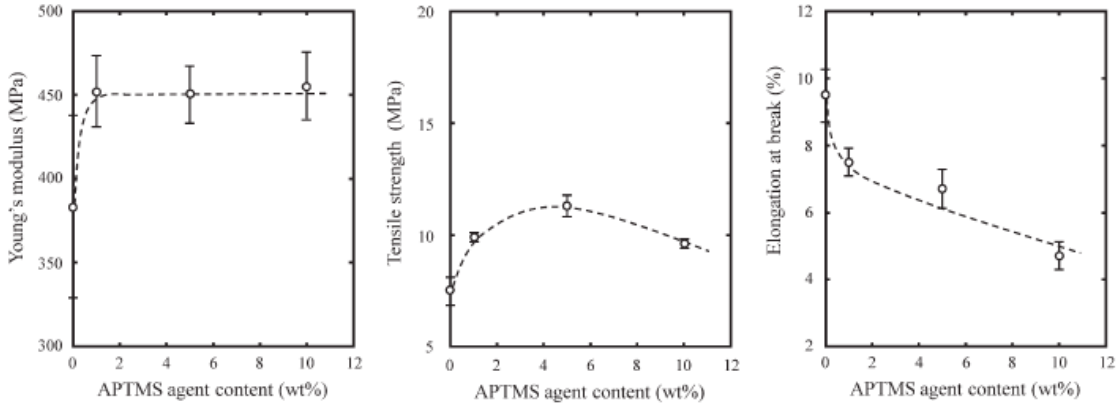

Fig.9 Young's moduli, tensile strengths, and elongations at break of the SPP ((70 - x) wt %)/SPP-g-DMI (x wt %)/ HC (30 wt %).

silane agent must be considerably less. In fact, as shown in Table III, the Si content of the silanized HC with the APTMS is around 1.5 mol% regardless of the APTMS concentration. The less dependence of the concentration on the Si content suggests that the reactivity of the OH group in the HC is much less than that in the FC.

Young's moduli, tensile strengths and elongations at break of the SPP (70 wt %)/silanized HC (30 wt %) with various content of APTMS are shown in Figure 8. In the cases of the Young's modulus and the tensile strength of the SPP/silanized HC with the 1 wt % content, these values increase ~ 18% and ~ 30%, respectively, as compared with those of the SPP/HC. These behaviors suggest

that the interface between the SPP and the HC is considerably reinforced even by the small formation of the covalent bond (-Si-O-C-). As shown in Figure 8, these values are almost constant up to the 10 wt % content, suggesting that the amount of the covalent bond does not change with the increase of the APTMS content. It seems that most of an active OH group in the HC reacts with the APTMS at the 1wt %. The APTMS in excess of the 1 wt % hardly works as the coupling agent. Whereas, the elongations at break quickly decrease with the increase of the APTMS content (see Fig. 8), suggesting that the embrittlement of the SPP matrix is developed by the excess of the APTMS. Young's moduli, tensile strengths and elongations at break of SPP ((70 - x) wt %)/SPP-g-DMI (x wt %)/HC (30 wt %) are shown in Figure 9. The Young's moduli and the tensile strengths gradually increase with the increase of the SPP-g-DMI content.

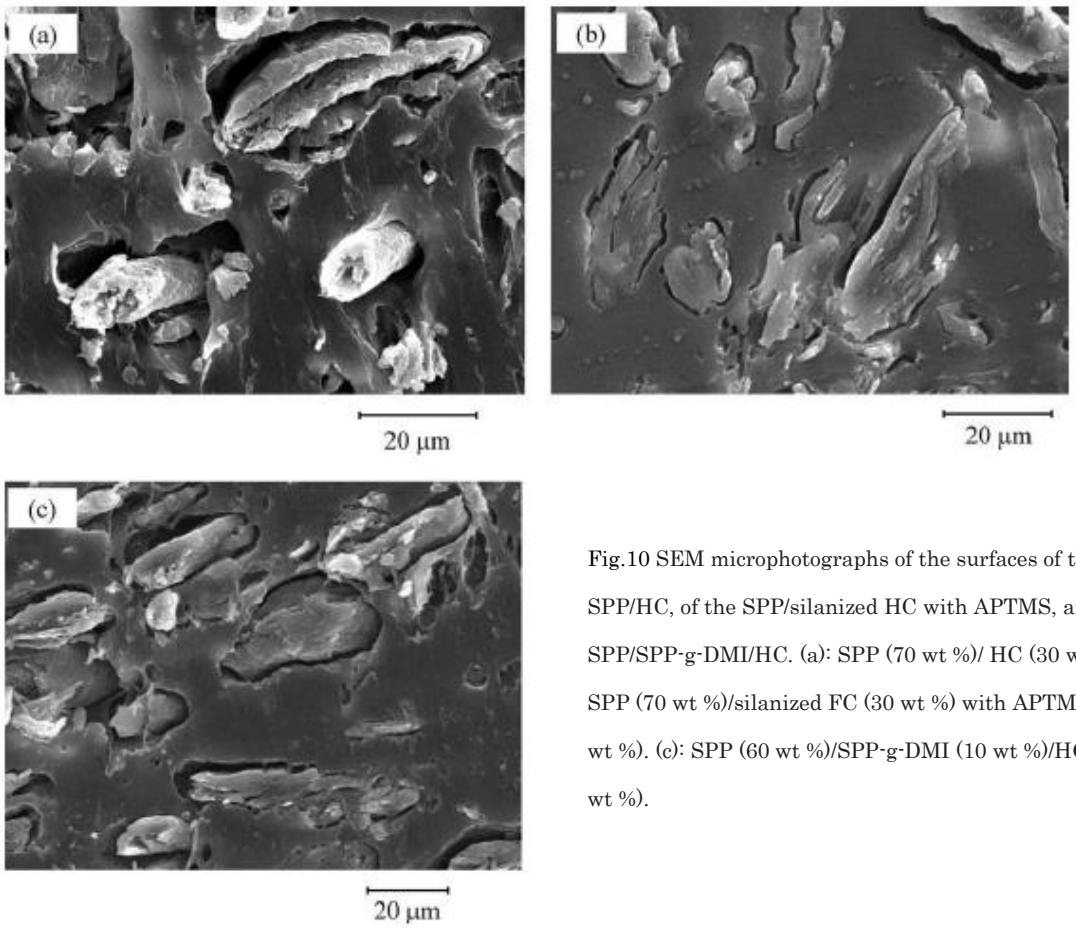

Fig.10 SEM microphotographs of the surfaces of the SPP/HC, of the SPP/silanized HC with APTMS, and of the SPP/SPP-g-DMI/HC. (a): SPP (70 wt %)/ HC (30 wt %). (b): SPP (70 wt %)/silanized FC (30 wt %) with APTMS (10 wt %). (c): SPP (60 wt %)/SPP-g-DMI (10 wt %)/HC(30 wt %).

Whereas, the elongations at break gradually decrease with the increase of the SPP-g-DMI content. These dependences are similar to those in SPP/SPP-g- DMI/FC and are, however, much lower. These results suggest that the reactivity with the OH group on the HC is considerably low as well as the APTMS.

Figure 10 shows the SEM microphotographs of the surfaces of the SPP/HC, the SPP/silanized HC with the APTMS, and the SPP/SPP-g-DMI/HC, respectively. As shown in Figure 10(a), large voids exist between the HC and the SPP matrix, suggesting that the interfacial adhesion is very poor as well as that of the SPP/FC. In the cases of the SPP/silanized HC with the APTMS and of the SPP/SPP-g-DMI/HC, the size of the voids dramatically decreases as well as those of these FC samples (see Fig. 3), indicating that the interfacial adhesions are certainly improved. However, these boundaries between the HC and the SPP matrix are considerably distinct, demonstrating that the interfacial adhesion is considerably weak.

2-4 Conclusions

The reinforcement of the interfacial adhesion between the SPP and the FC was performed by the FC silanizations with the APTMS and the HTMS and by the addition of the SPP-g-DMI graft-polymer, respectively. It was confirmed that the interfacial adhesion was certainly improved by them. However, the reinforcement behavior was considerably different among these methods. In particular, the FC silanization with the HTMS showed the specific tensile behavior. The existence of the hexyl group in the HTMS led to the block of the inter hydrogen bonding in the FC. Therefore, the cohesion force among the celluloses became weaker with the increase of the degree of the silanization, and the silanized FC was embrittled. In the case of the APTMS, the

hydrogen bonding among the celluloses was kept because of the existence of the amino group. Whereas, the SPP-g-DMI was unable to penetrate into the celluloses because of its higher molecules, and the inter hydrogen bonding was not blocked. It was found that the keeping the inter hydrogen bonding among the celluloses was important for the reinforcement of the tensile properties such as Young's modulus and tensile strength in the SPP/ FC composite.

In addition, to study the reactivity with HC which is the mixture of cellulose and hemicellulose, the SPP/silanized HC with the APTMS and the SPP/ SPP-g-DMI/HC were prepared and, the tensile behavior and the morphology were studied. The Young's moduli and the tensile strengths were considerably improved by the APTMS silanization and by the addition of the SPP-g-DMI, respectively. Whereas, these improvements hardly showed dependency on the APTMS content and the SPP-g-DMI amount. The behavior suggested that the each of reactivities with the OH group in the HC were considerably low. In the SEM observations of the SPP/silanized HC with the APTMS and the SPP/SPP-g-DMI/ HC, it was confirmed that these interfacial adhesion was certainly improved. However, these boundaries between the HC and the SPP matrix were considerably distinct, demonstrating that the interfacial adhesion was considerably weak. It was found that the reactivity of the HC was much less than that of the FC composing of pure cellulose.

References

1. S. Takase, N. Shiraishi,. *J. Appl. Polym. Sci.* **1989**, 37, 645.

2. D. Maldas, B. V. Kokta, C. Daneault,. *J. Appl. Polym. Sci.* **1989**, 37, 751.

3. R.J. Raj, B. V. Kokta, D. Maldas, C. Daneault,. J Appl Polym Sci **1989**, 37, 1089.

4. P. Hedenberg, P. Gatenholm,. *J. Appl. Polym. Sci.*, **1996**, 60, 2377.

5. F. Zhang, W. Qiu, L. Yang, T. Endo., *J. Mater. Chem.* **2002**, 12, 24.

6. W. Qiu, F. Zhang, T. Endo, T. Hirotsu., *J. Appl. Polym. Sci.* **2003**, 87, 337.

7. W. Qiu, F. Zhang, T. Endo, T. Hirotsu., *J. Appl. Polym. Sci.* **2004**, 91, 1703.

8. J. M. Felix, P. Gatenholm., *J. Appl. Polym. Sci.* **1991**, 42, 609.

9. W. Qiu, F. Zhang, T. Endo, T. Hirotsu., *J. Appl. Polym. Sci.* **2004**, 94, 1326.

10. V. N. Hristov, S. T. Vasileva, M, Krumova, R. Lach, G. H. Michler., *Polym. Compos.* **2004**, 25, 521.

11. R. Karnani, M. Krishnan, R. Narayan., *Polym. Eng. Sci.* **1997**, 37, 476.

12. H. Nakatani, K, Hashimoto, K. Miyazaki, M. Terano., *J. Appl. Polym. Sci.* 2022 **2009**, 113.

13. S. M. Kanan, W. T. Y. Tze, C. P. Tripp., *Langmuir* **2002**, 18, 6623.

14. E. A. Smith, W. Chen., *Langmuir* **2008**, 24, 12405.

15. L. M. Matuana, J. J. Balatinecz, C. B. Park, R. N. S. Sodhi., *Wood Sci. Technol.* **1999**, 33, 259.

16. L. E. Wise, E. C. Jahn., *Wood Chemsitry*, 2nd ed., Reinhold Publishing, New York, **1952**.

17. M. Yazdani-Pedram, H. Vega, R. Quijada., *Polymer* **2001**, 42, 4751.

18. H. Nakatani, K. Iwakura, K. Miyazaki, N. Okazaki, M. Terano, *J. Appl. Polym. Sci.* **2011**, 119, 1732.

19. K. Miyazaki, K. Moriya, N. Okazaki, M. Terano, H. Nakatani., *J. Appl. Polym. Sci.* **2009**, 111, 1835.

Chapter 3

Syndiotactic Polypropylene/Microfibrous Cellulose Composites: Effect of Filler Size on Tensile Properties

3-1: Introduction

Cellulose has been one of most popular polymeric materials in the world and is much attractive in low cost, high modulus, renewable, and biodegradability. The structure of cellulose is a branched linear polymer with a high degree of hydrogen bonding. [1] The crystal structure is mainly composed of cellulose-I crystal form with a parallel conformation of two anyhydroglucose units joined by a single b-D glycosidic linkage.[2] Some work has also found that cellulose-I is composed of a mixture of two crystal forms, namely cellulose-I-a and -I-b.[3,4] The crystal deformation behavior has been studied with compacted specimens of a large number of microcrystalline cellulose particles. [5,6] Commercially, cellulose has attracted much attention as filler material because of its high-modulus.[7–25] The composite brings about the improvement of stiffness for pristine polymer. Recently, micro- and/or nano-sized cellulose such as microfibrous cellulose (MFC) and cellulose whisker has been studied as the new filler material by many investigators.[17–25] The micro (nano) cellulose filler has an ability to produce the composite with a higher modulus and/or good transparency. In fact, cellulose is hydrophilic and tends to aggregate in hydrophobic polymer such as polypropylene (PP), causing poor processability and incompatibility. It is very difficult to prepare the compatible micro cellulose composite. Therefore, systematic studies on the physical properties of the micro cellulose composite has been hardly performed.

The purpose of this study is to prepare a compatible polyolefin/ MFC composite and to study the dependence of tensile properties on the MFC loading content. Syndiotactic polypropylene (SPP) was used as the polyolefin material as it had good processability at a low temperature (150℃)[26,27] without occurrence of cellulose thermal degradation. However, a novel dispersion method has been required to obtain SPP/MFC composite

with good MFC dispersity because of the difference of polarity between both components. In order to prepare the compatible composite, ethanol has been used as surfactant. The MFC dispersity was evaluated by scanning electron microscope (SEM) measurement. The tensile properties were studied in comparison with those of the fibrous cellulose (FC) composite and of the theoretical value obtained from the Halpin-Tsai equation. In addition, the MFC loading effects on the crystallization and crystal morphology were studied by differential scanning calorimetry (DSC) and wide-angle X-ray diffraction (WAXD) measurements.

3-2: Experimental

3-2-1: Materials

SPP was supplied by Sanwayuka Industry Co. The trade name is TOTAL 1751. The number-average molecular weight (M_n) and the polydispersity (M_w/M_n) were 3.5×10^4 and 3.0, respectively. MFC (KY-100 G: solid paste state (dried MFC/water . 10 wt %/90 wt %)) was purchased from Daicel FineChen Ltd. The fiber diameter of the MFC is 10–100 nm (see Figure 1). The length is about 1–10 μm. FC (W-100GK) was donated by Nippon Paper Chemicals. The FC was dried in desiccator for 7 days before preparation. The moisture of the FC was below 0.7 wt %. The FC dimensions are over 90 wt % pass 100 mesh (below 150 μm), the average length was about 37 μm. Ethanol was purchased from Wako Pure Chemical Industry, respectively.

3-2-2: Preparations of MFC Samples

Two kinds of the MFC were used in this study. They were named as “MFC” and

“ethanol swelled MFC,” respectively. The MFC (KY-100 G) was solid paste containing water as mentioned above. The preparation of the ethanol swelled MFC was as follows: The MFC was poured into a lot of ethanol solvent and was vigorously stirred. The MFC exchanged was separated from ethanol solvent by a suction filtration and was in a solid paste state (MFC/ethanol = 10 wt %/90 wt %). The ethanol swelled paste was used as “ethanol swelled MFC” in this study.

3-2-3: Preparation of Composites

Composites are prepared by an Imoto Seisakusyo IMC-1884 melting mixer. All mixtures (total weight 5 g) were carried by each weight ratio. After a small amount of phenolic antioxidant (Adekastab AO-60, ca. 0.5%) was added, the mixing was performed at 150℃ at 60 rpm for 5 min except the SPP/ethanol swelled MFC composite. In the case of the SPP/ethanol swelled MFC composite, the mixing was performed at 165℃ at 60 rpm for 10 min because the ethanol volatilization brought about the decrease of the mixing temperature. First, the SPP was put into the melting mixer, and then the MFC ethanol solid paste was added with letting the ethanol vapor out. The composites obtained were molded into the film (100 μm) by compression molding at 150℃ under 40 MPa for 5 min.

3-2-4: Scanning Electron Microscope Observation

SEM observation was carried out with a JEOL JSM-5800 at 20kV. The composite was molded into the plate (ca.500 μm) by compression molding at 150℃ under 40 MPa for 5 min. The plate obtained was fractured in liquid nitrogen, was trimmed by a microtome, and then the fractured surface was sputter-coated with gold.

3-2-5: Differential Scanning Calorimetry Measurement

DSC measurements were made with a Shimadzu DSC-60. The film (thickness: 100 μm) samples of about 2 mg weight were sealed in aluminum pans. The measurements of the samples were carried out at heating and cooling rates of 10℃/min under a nitrogen atmosphere, respectively. From the thermogram, melting temperature (T_m) and fusion enthalpy (ΔH) were determined. The crystallinity (Xc) of the SPP part in the composite was obtained by using the relationship:[28]

$$Xc = (\Delta H / \Delta H^{\circ}) \cdot (100/w) \quad (1)$$

where ΔH° =109.3 J/g for 100% crystalline SPP was taken,[29] and w is the mass fraction of SPP in the composite.

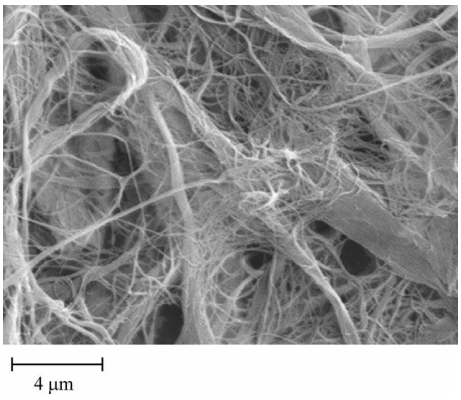

Fig. 1 SEM microphotograph of MFC.

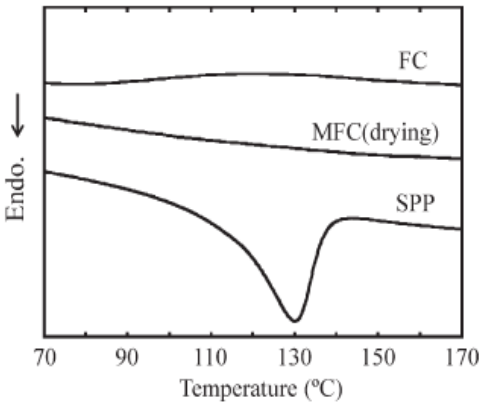

Fig. 2 DSC curves of heating scans for SPP, MFC(drying), and FC.

3-2-6: Wide-Angle X-ray Diffraction Measurement

WAXD diffractograms were recorded in reflection geometry at 2° (2 theta/min) under Ni-filtered Cu Ka radiation using a RIGAKUXG-RINT 1200 diffractometer. The MFC was molded into the film (100 μm) by compression molding at r.t. under 5 MPa for 7 min and then sufficiently dried at r.t. In the case of FC sample, the FC was sufficiently dried at r.t. without compression molding. They were measured by the WAXD device. These crystallinity values were estimated from the WAXD profiles according to Ant-Wuorinen's report.[30] The WAXD measurement of the composite was carried out with the 100 μm film.

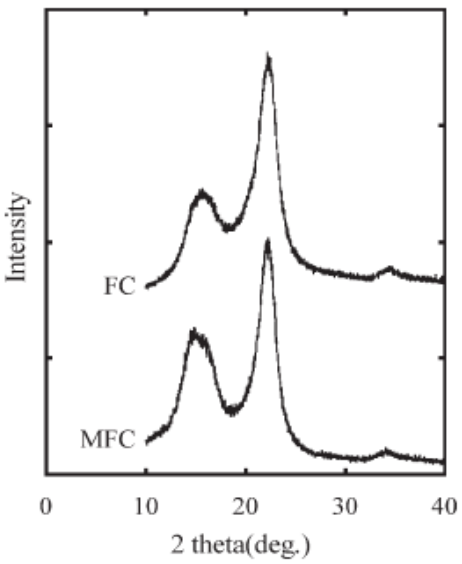

Fig. 3 WAXD profiles of MFC and FC.

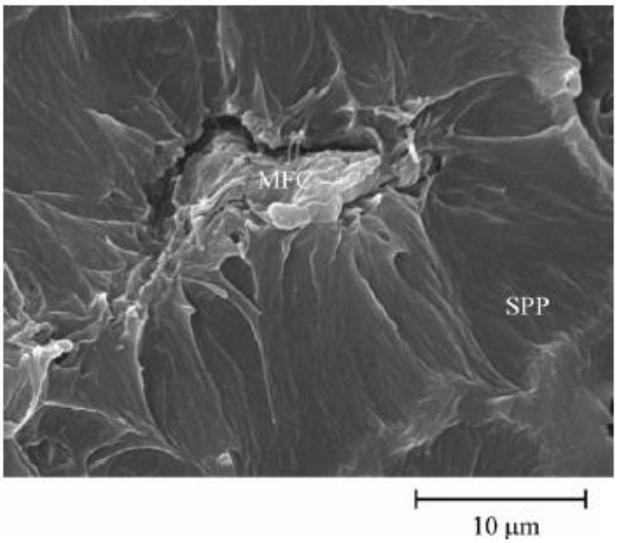

Fig. 4 SEM microphotographs of the surfaces of the SPP(98 wt %)/water swelled MFC(2 wt %).

3-2-7: Tensile Testing

Stress-strain behavior was observed using a SHIMADZU EZ-S at a cross-head speed of 3 mm/min. The sample specimens were cut with dimensions 30 × 5 × 0.1 mm shape in which the gage length was 10 mm. We chose the specialized specimen (like ISO

reed-shape) to adapt to the size of our tensile testing machine. All of tensile testing were performed at 20℃. The values of Young's modulus were obtained from the tangent slope of the stress-strain curve (until about 1% of the strain value). All results obtained were the average values of ten measurements.

3-3: Results and Discussion

Figure 2 showed the DSC curves of the SPP, MFC, and FC. The SPP melting temperature (T_m) is 130℃, and the other materials have no T_m. All materials have no exothermal peaks, showing pyrolysis does not occur up to 170℃. These results indicate that thermal deterioration of the cellulose materials does not occur under the composite preparation process. Figure 3 showed the WAXD profiles of the MFC and FC. Both of them show typical cellulose-I crystal form,[31] and their crystallinity values of the MFC and the FC are 62% and 53%, respectively.

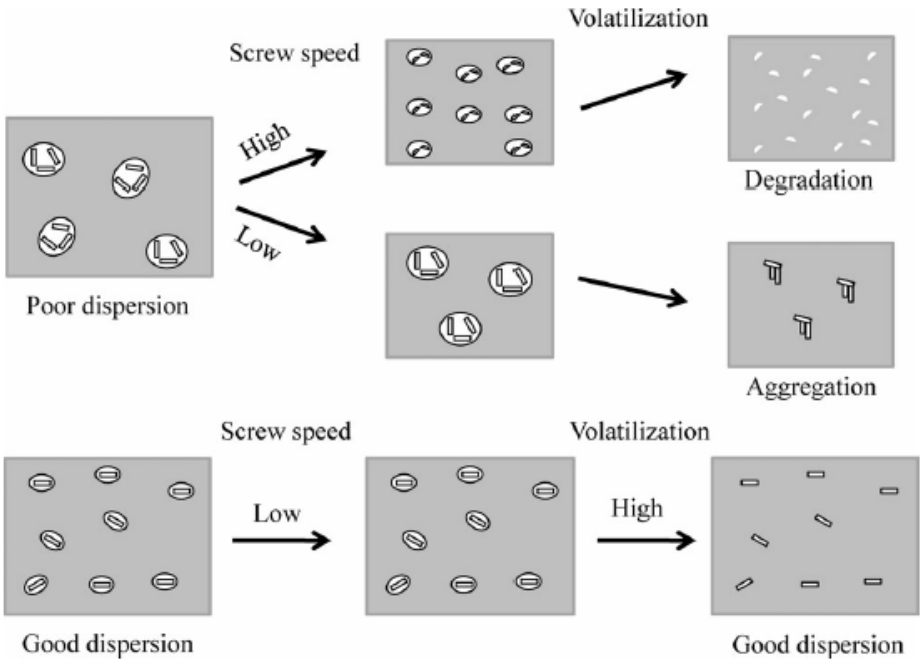

Fig. 5 Plausible mechanism of MFC dispersion in polyolefin using various lubricants.

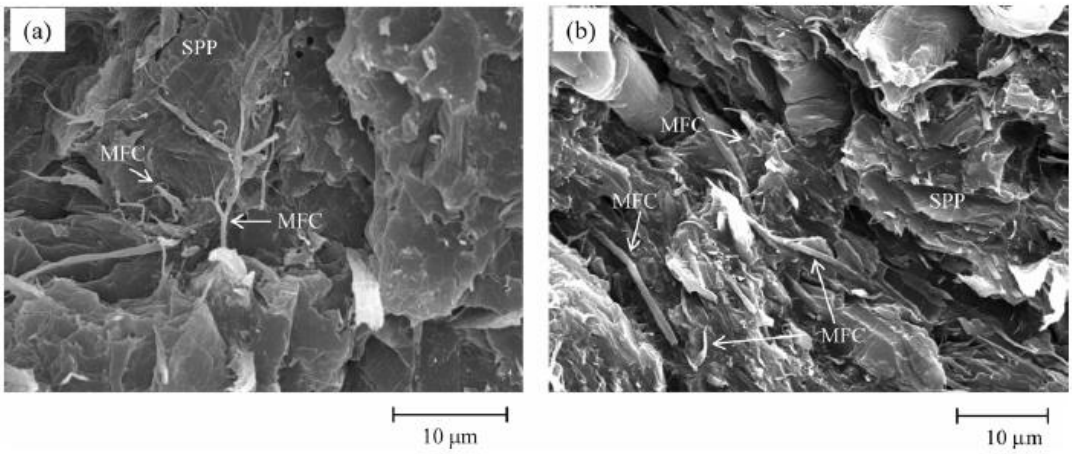

Fig. 6 SEM microphotographs of the surfaces of the SPP/ethanol swelled MFC. (a): SPP (80 wt %)/ethanol swelled (20 wt %). (b): SPP (60 wt %)/ ethanol swelled (40 wt %).

Figure 4 showed the SEM micrograph of the SPP(98 wt %)/ MFC(2 wt %) surface. An aggregated MFC (ca. 15 μm) can be also observed, and the interface between the MFC and SPP matrix is defined. In the melt mixing process, the presence of water acts as a lubricant and supports the MFC dispersion.[20] In this work, the effect is less due to the low screw speed (60 rpm). The water lubricant method requires high screw speed to obtain good MFC dispersity in polyolefin matrix such as polyethylene.[20] As shown in Figure 5, the requirement is due to low solubility of water against polyolefin, and the water lubricant brings about a phase separation structure in this melt mixing process. The water domain size certainly depends on the magnitude of shear stress produced by the screw. The larger domain includes many MFCs. After the water vaporization in the melt mixing process, the aggregated MFCs are left at the imprint of the domain, leading to the lower dispersity. Although the higher screw speed is desirable in terms of dispersity, it simultaneously brings about thermal deterioration of MFC.[20] As another method to get the good MFC dispersity, there is a surfactant application. Ljungberg et al. reported that phosphoric ester of polyoxyethylene-9-nonylphenyl ether (BNA) was useful as a surfactant to prepare PP/MFC composite showing a good MFC

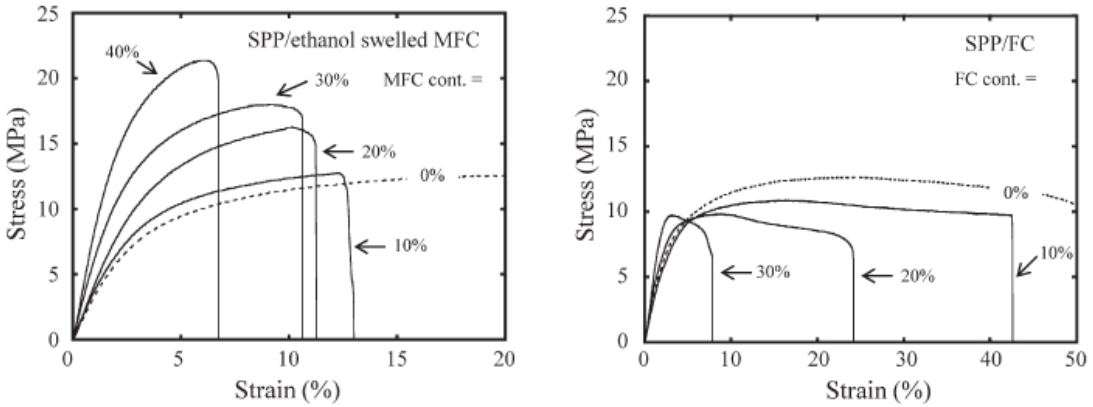

Fig. 7 Stress-strain curves of SPP/ethanol swelled MFC and SPP/FC composites with various cellulose filler content.

dispersity.[18,19] The BNA surfactant can bring about the good MFC dispersity even by cast film methods,[18,19] suggesting that it has an ability to produce the SPP/MFC composite with a welldispersed MFC even at the low screw speed. However, the BNA with such molecular weight would certainly remain in the SPP/ MFC composite and would affect the properties.[19] It is inappropriate to add much amount of such surfactant into the SPP/ MFC composite in terms of the properties such as tensile one.

A surfactant showing high volatility must be required to prepare the SPP/MFC composite with a high MFC content at low screw speed. As such surfactant, ethanol is considered because it is compatible for both of water and hydrocarbon and has a low boiling point (80℃) required for rapid volatilization. As shown in Figure 5, the application of the MFC ethanol solid paste has a potential for providing the good dispersity in the SPP matrix even at low screw speed. Figure 6 showed the SEM microphotographs of the surfaces of the SPP (80 wt %)/ethanol swelled MFC (20 wt %) and SPP (60 wt %)/ethanol swelled MFC (40 wt %). The aggregated MFC parts are not observed in both of the microphotographs. These results suggest that ethanol acts as a good surfactant for MFC.

All of the stress-strain curves of the SPP/ethanol swelled MFC and SPP/FC composites

were plotted in Figure 7. Figure 8 showed the plot of Young's modulus versus MFC or FC content (vol %) for the SPP composites. The Young's moduli of both of the SPP composites are increasing with the increase of the MFC or FC content. The effect of the MFC loading on the Young's modulus is higher than that of the FC one, and the values of the 6.1 vol % (10 wt %), 12.7 vol %(20 wt %) and (30 wt %) MFC content are 117, 140, and 117% higher than those of the FC, respectively. Effect of filler material on Young's modulus can be estmated by the Halpin-Tsai equation.[32–34]

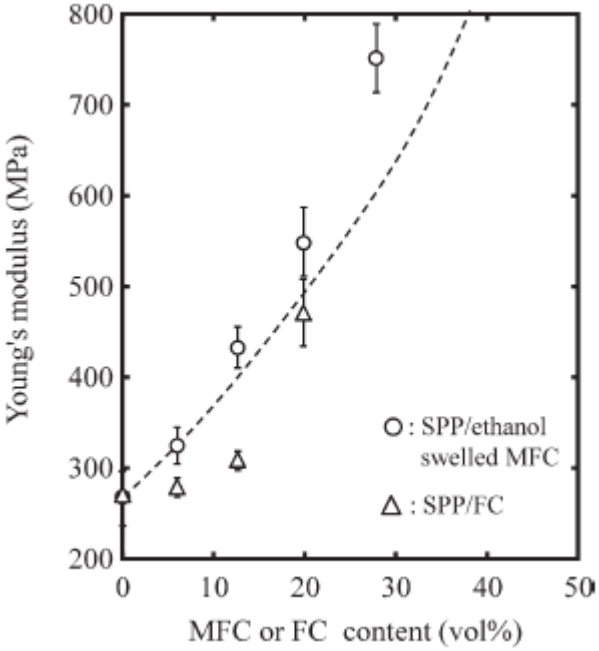

Fig. 8 Young's modulus of SPP composite against MFC or FC content (vol %). Broken curve: The Halpin-Tsai equation. MFC or FC . 10, 20, 30, and 40 wt % corresponding to . 6.1, 12.7, 19.9, and 27.9 vol %, respectively. Preparation of SPP (60 wt %)/FC (40 wt %)

$$M = M_1 \frac{1 + AB\phi}{1 - AB\phi} \tag{2}$$

in which

$$A = k_E - 1 \tag{3}$$

$$B = \frac{(M_2/M_1) - 1}{(M_2/M_1) + A} \tag{4}$$

where M, M_1, and M_2 are moduli of the composite, SPP matrix, and MFC or FC filler component, respectively; φ is the volume fraction (vol %) of component; k_E is the Einstein coefficient; A is the transference efficiency from the matrix to the filler. The M_1 (268 MPa) was directly obtained from the SPP sample, and the M_2 (9.2 GPa) was

assumed as Young's modulus of microcrystalline cellulose.6 k_E has a strong correlation with Poisson's ratio m. m of composite is approximately given by a mixture rule:[35]

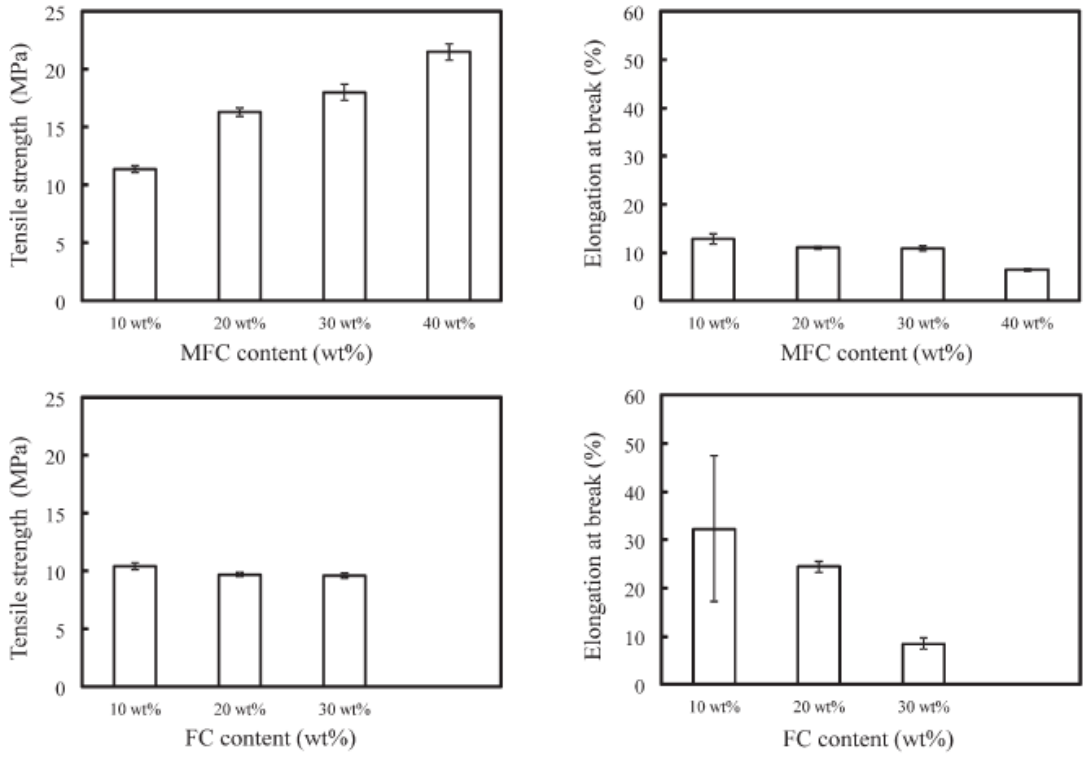

Fig. 9 Comparisons of tensile strengths and elongations at break of SPP/ethanol swelled MFC and SPP/FC composites with various cellulose filler content. The elongation at break of the SPP is 200% over. Preparation of SPP (60 wt %)/FC (40 wt %) composite was impossible.

$$v = v_m \phi_m + v_f \phi_f \tag{5}$$

where v_m and v_f are the Poisson's ratios of matrix (SPP) and filler (MFC or FC), respectively; φ_m and φ_f are the volume fractions of matrix and filler, respectively. The Poisson's ratios used in this approach having the following values: v_m . 0.38[36] and v_f = 0.30.[36] The v obtained is from 0.36 to 0.38. According to the data of Nielsen,[34] in a rigid matrix having near v value (0.35), the Einstein coefficient k_E was 3.81. Therefore, in this study, the m and the k_E have been regarded as 0.35 and 3.81, respectively, and the values of A and B have been estimated form eqs. (3) and (4). The Halpin-Tsai

equation obtained was plotted in Figures 8. Interestingly, the Young's moduli of the SPP/ethanol swelled MFC composites are higher than those of the Halpin- Tsai equation. The values of the 6.1 vol % (10 wt %), 12.7 vol % (20 wt %), 19.9 vol % (30 wt %), and 27.9 vol % (40 wt %) MFC content are 0.9%, 9.3, 12.2, and 23.9% higher than those of the Halpin-Tsai equation, respectively. The gap between the measured and Halpin-Tsai equation values is markedly increased with the increase of the MFC content. In contrast, the Young's moduli of the SPP/FC composites are lower than those of the Halpin-Tsai equation. The difference of the tensile behavior between the MFC and FC composites would be mainly originated from total interface surface area. The total surface area of the MFC is much larger than that of the FC because of the much smaller size (see Experimental section). Therefore, the total friction force acting on the MFC is much larger, and a shear stress from the SPP matrix is efficiently applied to the MFC filler. Figure 9 showed the comparisons of the tensile strengths and elongations at break of the SPP/ethanol swelled MFC and SPP/FC composites with various MFC or FC content. The tensile strength of the SPP/ethanol swelled MFC certainly increases with the increase of the MFC content, and the dependence of the elongation at break on the MFC content is less. It seems that the interfacial defect such as void is hard to produce. In contrast, the dependence of the tensile strength on the FC content is less, and the elongation at break rapidly decreases with increase of the FC content. The behavior suggests that the shear stress from the SPP matrix is inefficiently applied to the FC by blocking of the interfacial defect such as void. In fact, the SEM microphotograph of the SPP/FC showed that a large void existed between the FC and the SPP matrix. When the tensile stress is applied to the SPP/FC, the transmission of the applied stress is prevented by the void. The elongations at break of the 10 wt % and 20 wt % FC content

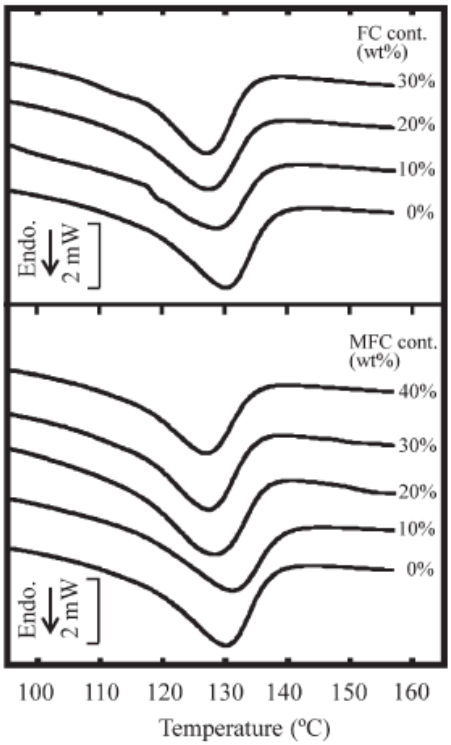

Fig. 10 DSC curves of heating scans for SPP/FC (top) and SPP/ethanol swelled MFC (bottom) composites. The numeric characters on the curves are FC or MFC wt % in composites. The endothermal peaks are corresponding to melting temperatures (T_m).

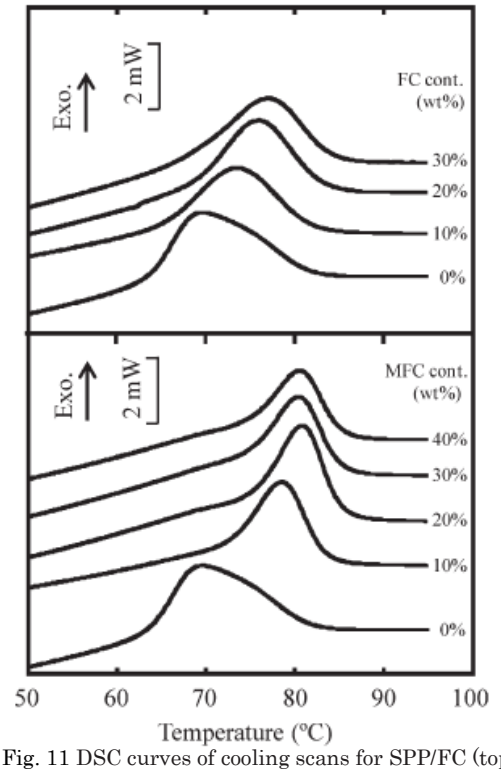

Fig. 11 DSC curves of cooling scans for SPP/FC (top) and SPP/ethanol swelled MFC (bottom) composites. The numeric characters on the curves are FC or MFC wt % in composites. The exothermal peaks are corresponding to crystallization temperatures (T_c).

are 32.3 ± 15.1% and 24. ± 1.2%, respectively and are considerably higher than those of the MFC composites with the same content. The deformation of only the SPP matrix occurs during the tensile testing in the SPP/FC, resulting that the SPP/FC shows the much greater elongation.

Table Ⅰ. Melting Temperature (T_m), Fusion Enthalpy (ΔH), Crystallinity (X_c), and Crystallization Temperature (T_c) of SPP/Ethanol Swelled MFC and SPP/FC Composites

MFC or FC cont. (wt %)	T_m (°C)	ΔH (J/g)	X_c (%)*	T_c (°C)
MFC				
0	130	24.4	22	69
10	131	22.9	23	78
20	128	27.3	31	81
30	127	25.1	33	81
40	127	20.4	31	81
FC				
10	129	24.3	25	74
20	127	23.2	27	76
30	127	24.1	32	77

*X_c was obtained from eq. (1) (see Experimental Part).

The Young's moduli of the SPP/ethanol swelled MFC composites exceed the theoretical ones obtained from the Halpin-Tsai equation. The phenomenon would be explainable in terms of an increase of the Young's modulus of the SPP matrix. Figures 10 and 11 showed the DSC curves around the melting (T_m) and crystallization (T_c) temperatures, respectively. These results were summarized in Table I. The Tm values are lowered from 130℃ to 127℃. The declining trend in Tm is exhibited up to the 20 wt % MFC or FC content, and then their Tm values are almost constant at 130℃. Interestingly, there is a difference between the ethanol swelled MFC and FC composites in the content dependence of the crystallinity (X_c). The X_c of the ethanol swelled MFC composite rapidly increases up to the 20 wt % content and then is saturated at about 31%. The T_c increasing tendency is similar to that of the X_c. The Young's modulus gap between the measured and Halpin-Tsai equation values is markedly increased with the increase of the MFC content. The X_c increment leads to an increase of the Young's modulus of the SPP matrix itself, causing the excessive increase of that of the SPP/ ethanol swelled MFC composite. It is well known that crystallinity and crystallization rate of polymer materials increase with nucleating agent effect.[28,37–39] Therefore, the X_c and T_c increment indicates that the MFC certainly acts as a nucleating agent for SPP. There is an interaction between cellulose and isotactic polypropylene (IPP) at a molecular level.[38] Cellulose surface has many the a-nucleation sites formed by the interaction, resulting that the IPP transcrystallization occurs.[38] It seems that the interaction acts as the a-nucleation site for the crystallization in SPP as well as IPP.28 In particular, the MFC has a good ability to act as the a-nucleation agent because of its large total surface area. As shown in Figure 12, the main peaks corresponding to SPP crystal form in the profiles of the SPP/ethanol swelled MFC composites are at 2θ = 12.2°, 15.9°, and 20.6°

(corresponding to orthorhombic a-form (Form I)),[40] respectively, and their peak location coincides with that of the pristine SPP. The WAXD profiles suggest that the MFC has only the a-nucleating effect on SPP. The MFC existence induces the a-form crystallization of a less crystallizable part in the SPP matrix, resulting that the SPP crystals with a lower degree of perfection, i.e., thicker lamellar, is produced. The apparent T_m shifts to a lower temperature by the increase in population of such SPP crystals. A degree of lowering of the apparent T_m reflects the α-nucleating effect. The a-nucleation effect such as the X_c and T_c increment is saturated over the 20 wt % MFC loading content. The aturation behavior is originated from the microstructured (nanostructured) cellulose surface since the FC with less total surface area does not show it. The population of the a-nucleation site at the 20 wt % MFC content reaches a concentration sufficient to crystallize all of crystallizable SPP part. The higher deviation from the Halpin-Tsai equation is originated from the Young's modulus change of the SPP matrix induced by the crystallinity change from 22% to 31%. It is found that the loading of the MFC brings about the Young's modulus improvement of the SPP with both of the higher modulus of MFC itself and the α-nucleating effect for the matrix.

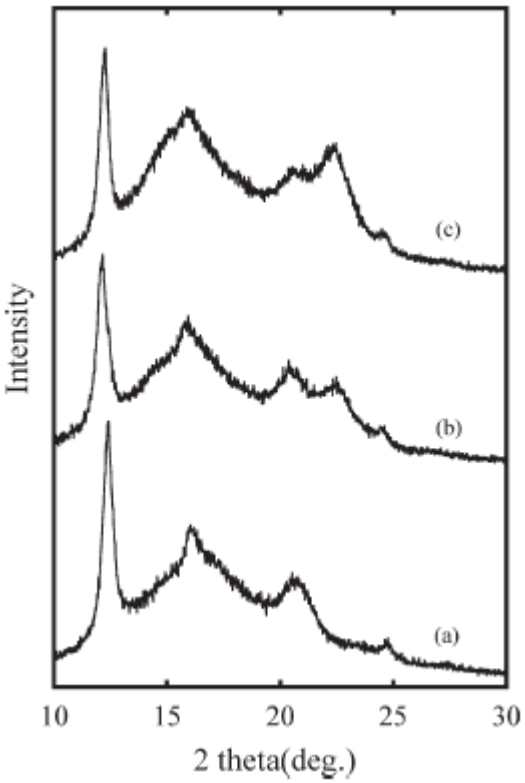

Fig. 12. WAXD profiles of SPP and SPP/ethanol swelled MFC composites. (a): SPP. (b): SPP (80 wt %)/ethanol swelled (20 wt %). (c): SPP (60 wt %)/ethanol swelled (40 wt %).

3-4: Conclusions

The morphology and tensile properties of the SPP/ethanol swelled MFC composite were studied as compared with those of the SPP/FC one. The aggregated MFC part was not observed in the SEM microphotographs, and the Young's modulus of the composite was exponentially increasing with the increase of the MFC content. These results suggested that the MFC was welldispersed in the SPP matrix by ethanol surfactant. The effect of the MFC loading on the Young's modulus was much higher than that of the FC one. The Young's modulus of the SPP/ ethanol swelled MFC composite exceeded the theoretical one obtained from the Halpin-Tsai equation. The MFC acted as a good a-nucleation agent for SPP because of its large total surface area. The excessive Young's modulus of the MFC composite was originated from an increase of that of the SPP matrix induced by the a-nucleation effect.

References

1. S. J. Eichhorn, R. J. Young, *Cellulose.* **2001**, 8, 197.

2. R. H. Marchessault, Sundararajan, P. R. The Polysaccharides, *Cellulose*, Aspinall G. O., Eds.; Academic Press: New York, **1983**; *Vol.* 1, pp 12–90.

3. R. H. Atalla, D. L. Van der Hart., *Science* **1984**, 223, 283.

4. D. L. Van der Hart, R. H. Atalla., *Macromolecules* **1984**, 17, 1465.

5. S. Edge, D. Fraser Steele, A. Chen, M. J. Tobyn, J. N. Staniforth., *Int. J. Pharm.* **2000**, 200, 67.

6. B. C. Hancock, S.-D Clas, K. Christensen., *Int. J. Pharm.* **2000**, 209, 27.

7. S. Takase, N. Shiraishi., *J. Appl. Polym. Sci.* **1989**, 37, 645.

8. D. Maldas, B. V. Kokta, C. Daneault., *J. Appl. Polym. Sci.* **1989**, 37, 751.

9. R. G. Raj, B. V. Kokta, D. Maldas, C. Daneault., *J. Appl. Polym. Sci.* **1989**, 37, 1089.

10. P. Hedenberg, P. Gatenholm., *J. Appl. Polym. Sci.* **1996**, 60, 2377.

11. F. Zhang, W. Qiu, L. Yang, T. Endo., *J. Mater. Chem.* **2002**, 12, 24.

12. W. Qiu, F. Zhang, T. Endo, T. Hirotsu., *J. Appl. Polym. Sci.* **2003**, 87, 337.

13. W. Qiu, F. Zhang, T. Endo, T. Hirotsu., *J. Appl. Polym. Sci.* **2004**, 91, 1703.

14. J. M. Felix, P. Gatenholm., *J. Appl. Polym. Sci.* **1991**, 42, 609.

15. W. Qiu, F. Zhang, T. Endo, T. Hirotsu., *J. Appl. Polym. Sci.* **2004**, 94, 1326.

16. V. N. Hristov, S. T. Vasileva, M. Krumova, R. Lach, G. H. Michler., *Polym. Compos.* **2004**, 25, 521.

17. M. Grunert, W. T. Winter, *J. Polym. Env.* **2002**, 10, 27.

18. N. Ljungberg, C. Bonini, F. Bortolussi, C. Boisson, L. Heux, J. Y. Cavaille., *Biomacromolecules* **2005**, 6, 2732.

19. N. Ljungberg, J. Y. Cavaille, L. Heux., *Polymer* **2006**, 47, 6285.

20. J. Soulestin, N. Qui_evy, M. Sclavons, M. Devaux., *J. Polym. Eng. Sci.* **2007**, 47, 467.

21. D. G. Gray., *Cellulose* **2008**, 15, 297.

22. A. J. De Menezes, G. Siqueira, A. A. S. Curvelo, A. Dufresne., *Polymer* **2009**, 50, 4552.

23. H. S. Yang, D. J. Gardner, J. W. Nader., *J. Therm. Anal. Calori* **2011**, 103, 1007.

24. H. S. Yang, D. J. Gardner., *Wood Fiber Sci.* **2011**, 43, 143.

25. H. S. Yang, D. J. Gardner., *Wood Fiber Sci.* **2011**, 43, 215.

26. H. Nakatani, K. Iwakura, K. Miyazaki, N. Okazaki, M. Terano., *J. Appl. Polym. Sci.* **2011**, 119, 1732.

27. H. Nakatani, K. Iwakura, M. Hamadate, N. Okazaki, M. Aoyama, M. Terano., *J. Appl. Polym. Sci.* **2011**, 122, 2798.

28. A. Amash, P. Zugenmaier., *Polym. Bull.* **1998**, 40, 251.

29. P. Supaphol, J. E. Spruiell, J. Lin, J.-S. *Polym. Int.* **2000**, 49, 1473.

30. A. W. Ant-Wuorinen, Visapaa, A. *Norelco Reptr* **1962**, 9, 48.

31. A. Ishikawa, T. Okano, J. Sugiyama., *Polymer* **1997**, 2, 463.

32. Halpin, J. C. *J. Compos. Matter* **1969**, 3, 732.

33. T. B. Lewis, Nielsen, L. E. *J. Appl. Polym. Sci.* **1970**, 14, 1449.

34. Nielsen, L. E. *J. Appl. Phys.* **1970**, 41, 4626.

35. W. Helbert, J. Y. Cavaill_e, Dufresne, A. *Polym. Compos.* **1996**, 17, 604.

36. L. E. ASP, Sj€ogren, B. A.; Berglund, L. A. *Polym. Compos.* **1997**, 18, 9.

37. D. Kaempfer, R. Thomann, Mu¨lhaupt, R. *Polymer* 2002, 43, **2909**.

38. J. M. Felix, Gatenholm, P. *J. Mater. Sci.* **1994**, 29, 3043.

39. T. Xua, H. Lei, Xie, C. S. *Mater. Des.* **2003**, 24, 227.

40. C. De Rosa, F. Auriemma, Vinti, V. *Macromolecules* **1997**, 30, 4137.

Chapter 4

Additive effects of tripalmitin and low-density polyethylene on morphologies and tensile properties of polybutene-1/micro fibrous cellulose composite

4-1 Introduction

Cellulose has been one of the most popular polymeric materials in the world and has been used as raw materials of commercial materials for a long time ago. It has attracted much attention as a composite material [1–4] since it has great potential for the preparation of composite materials having high-modulus and renewability. As most popular composite based on cellulose, the composite with polyolefin has been extensively investigated by many researchers [1–7]. In particular, polypropylene (PP) and polyethylene (PE) have been often employed as the raw materials, and the tensile properties and morphologies of their cellulose composites have been studied in detailed. However, the composite with other polyolefin such as polybutene-1 (PB) has been little studied. Recently, Afrifah et al. [8] reported that the PB/ cellulose composite showed processability, elongation at breaks, impact strength and adhesion superior to those of the PP/- and PE/cellulose composites. These unique properties are due to specific feature of PB. It is polymorphic and has mainly two kinds of crystalline form [9–19]. One is the stable hexagonal crystal form (I), the other is the metastable tetragonal one (II). It spontaneously exhibits a crystal phase transformation from II to I crystal forms [9–19].

In our previous work, we have succeeded in the preparation of PB/MFC composite with a good dispersity by tripalmitin (TP) [20]. TP is a kind of plant wax and is the triglyceride of palmitic acid. The molecular structure is composed of three hydrophobic hexadecanyl chains and hydrophobic triglyceride group linking the chains. It is crystallizable and has a melting point (>65℃) [21]. These characteristics provide miscibility with butterfat, and the TP/butterfat blend shows barrier properties with respect to moisture [22]. It worked as compatibilizer between PB and micro fibrous

cellulose (MFC) because of the amphipathicity, and its loading provided a good dispersibility and ductility enhancement for PB/MFC composite [20]. However, effects of the loading on the tensile properties of the PB/MFC during the PB crystal phase transformation have not been clarified yet.

The purpose of the present work has been to clarify effects of the TP loading on the tensile properties of the PB/MFC with various MFC content during the PB crystal phase transformation. In addition, the effects of low-density polyethylene (LDPE) loading on the tensile properties of the PB/MFC have been studied as well as those of the loading since LDPE and PB polymer blend have commercially used as peel film materials [23]. In this study, the behavior of the crystal phase transformation has been studied by wide-angle X-ray diffraction (WAXD) measurement. The morphologies, the tensile and thermal decomposition properties have been by scanning electron microscope (SEM) and tensile testing, respectively.

4-2 Experimental

4-2-1 Materials

Pb was supplied by Mitsui Chemicals, Inc. The density was 0.915 g/cm^3, and melt flow rate (MFR) was 1.8 g/10 min. TP was purchased from Wako Pure Chemical Industry. LDPE was purchased from Sigma-Aldrich Co. LLC. The density was 0.925 g/cm^3, and melt index (MI) was 25 g/10 min. These were used without further purification. MFC [KY-100G: solid paste state (dried MFC/water = 10/ 90 wt%)] was purchased from Daicel FineChen Ltd. The fiber diameter of the MFC is 10–100 nm. The MFC (KY-100G) was solid paste containing water as mentioned above. The preparation of the

ethanol swelled MFC was as follows: The MFC was poured into a lot of ethanol solvent and was vigorously stirred. The MFC exchanged was separated from ethanol solvent by a suction filtration and was in a solid paste state (dried MFC/ethanol = 10/90 wt%). The ethanol swelled paste was employed as “MFC” in this study.

4-2-2 Preparations of polymer blend and composite

Polymer blends (PB/TP and PB/LDPE) were prepared by an Imoto Seisakusyo IMC-1884 melting mixer. All mixtures were carried by each weight ratio. After a small amount of phenolic antioxidant (Adekastab AO-60, ca. 0.5 %) was added, all mixing was performed. The mixing of the PB and TP or LDPE was performed at 150 ℃ at 60 rpm for 5 min. The blends obtained was molded into the film by compression molding at 150 ℃ under 10 MPa for 5 min and then were quickly quenched into a water bath. Polymer composites (PB/MFC, PB/TP/MFC and PB/LDPE/MFC) were prepared by the same melting mixer. All mixtures were performed by each weight ratio. After a small amount of phenolic antioxidant (Adekastab AO-60, ca. 0.5 %) was added, all mixing was performed. The mixing was performed at 150 ℃ at 60 rpm for 5 min. The composites obtained were molded into the film by compression molding at 180 ℃ under 10 MPa for 5 min and then were quickly quenched into a water bath.

4-2-3 SEM observation

SEM observation was carried out with a JEOL JSM-5800 at 20 kV. The plate (thickness: 500 μm) samples were fractured in liquid nitrogen, and then the fractured surfaces were sputter-coated with gold.

4-2-4 Tensile testing

Stress–strain behavior was observed using a SHIMADZU EZ-S at a cross-head speed of 3 mm/min. The sample specimens were cut with dimensions 30 × 5 × 0.1 mm shape in which the gauge length was 10 mm. We chose the specialized specimen (like ISO reed-shape) to adapt to the size of our tensile testing machine. All of tensile testing was performed at 20 ℃. The values of Young's modulus were obtained from the slope of the stress–strain curve (until about 1 % of the strain value). All results obtained were the average values of three measurements.

4-2-5 WAXD measurement

WAXD diffractograms of the film (thickness: 100 μm) samples were recorded in reflection geometry at 2°(2θ/min) under Ni-filtered Cu Ka radiation using a RIGAKUXG-RINT 1200 diffractometer.

4-3 Results and discussion

Figure 1 shows the SEM microphotograph of MFC. The fiber diameter of the MFC is 10–100 nm, and the fibers get entangled with each other. The microphotograph of fractured surface of the PB/MFC (10 %) shows the MFC entanglement. Although large aggregation of the MFC hardly occurs, it seems that the dispersity in PB is not so well [20].

Figure 2 shows the Young's moduli and of PB/MFC with various MFC loading and those of their aged ones. In previous study [24], loading of an ordinary size (ca. 100 μm) fibrous cellulose brought about an increase (ca. 150 %) of the Young's

modulus. The MFC loading brings about the higher increment. For example, the value increases up to ca. 760 % at the 50 % loading without the aging treatment. PB crystal phase transformation from the metastable tetragonal (II) to the stable

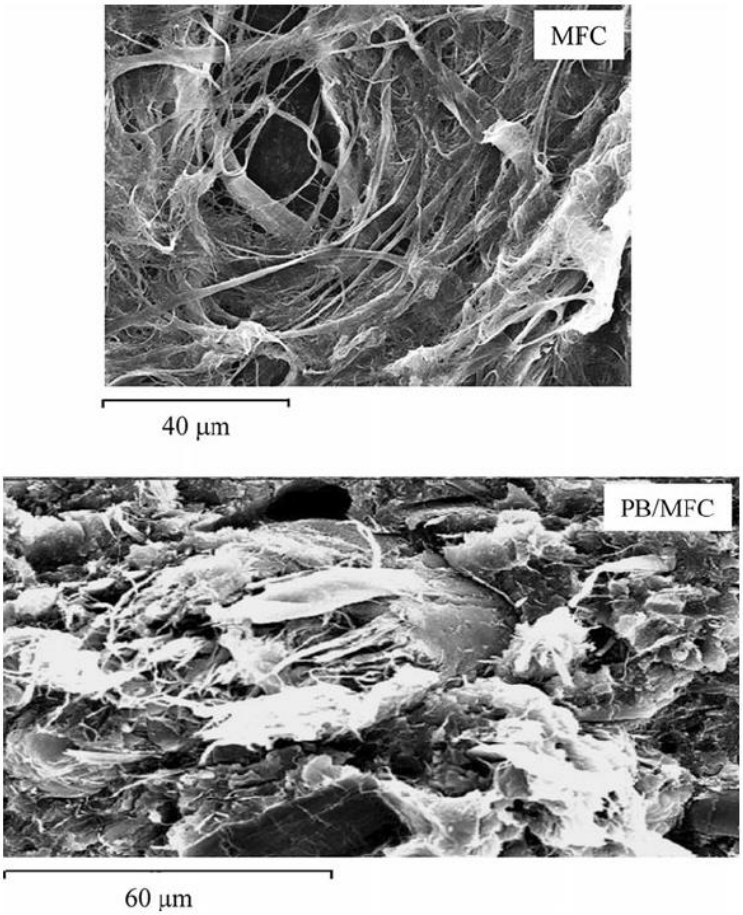

Fig. 1 SEM microphotographs of MFC and fractured surface of PB/MFC: MFC loading = 10 wt%/PB

hexagonal (I) one is certainly caused by the aging, leading to the Young's modulus increment [24]. Interestingly, the loading and crystal phase transformation work synergistically in increasing the Young's modulus. As shown in Fig. 3, however, they simultaneously bring about the rapid embrittlement because of poor interface strength between the PB and MFC.

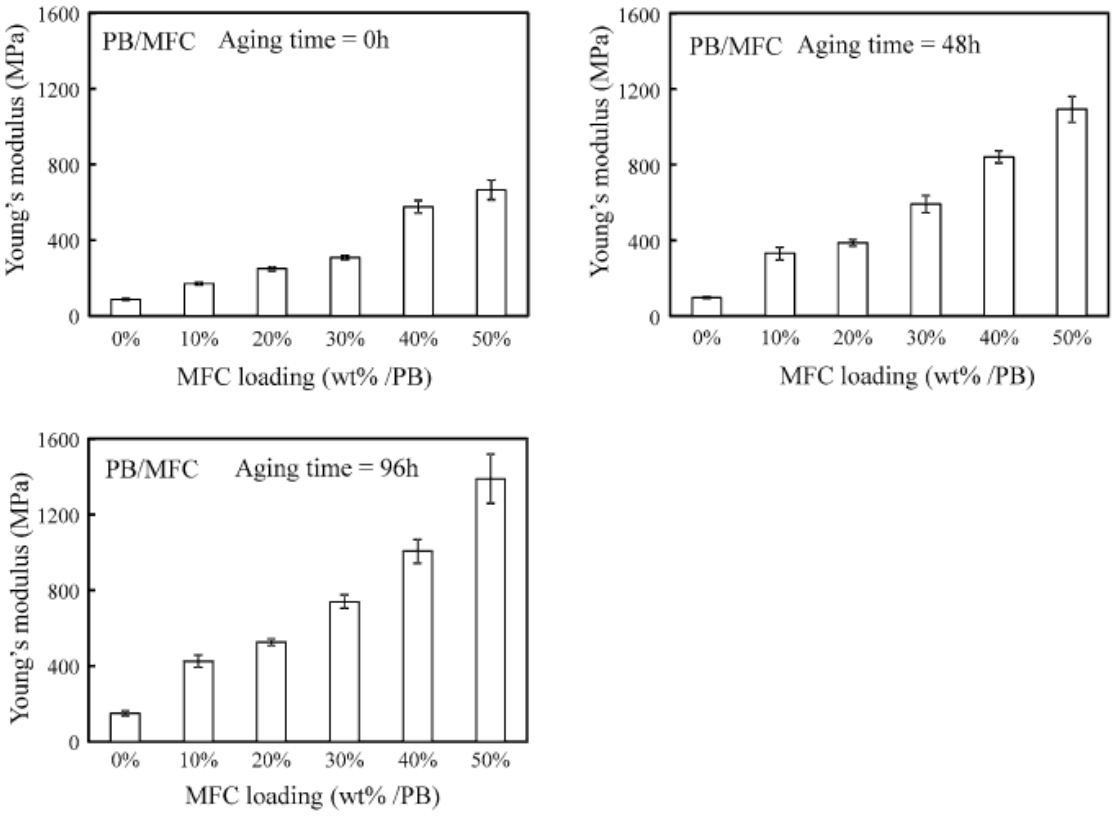

Fig. 2 Comparison of Young's moduli of PB/MFC films and their aged ones. Aging temperature = r. t.(ca. 20℃)

Figure 4 shows the SEM microphotograph of fractured surface of the PB/TP (10 %)/MFC (10 %). Overall, there is difficulty in viewing the MFC clearly, however, the isolated fibers can be certainly observed. The dispersibility is certainly improved by the TP, showing that the TP works as a good compatibilizer for the PB/ MFC composite [20]. Figure 5 shows the Young's moduli of the PB/TP (10 %)/ MFC with various MFC loading and those of their aged ones. The loading brings about the increment as well as the PB/MFC. The values are approximately 90 % of those of the PB/MFC up to 20 % MFC

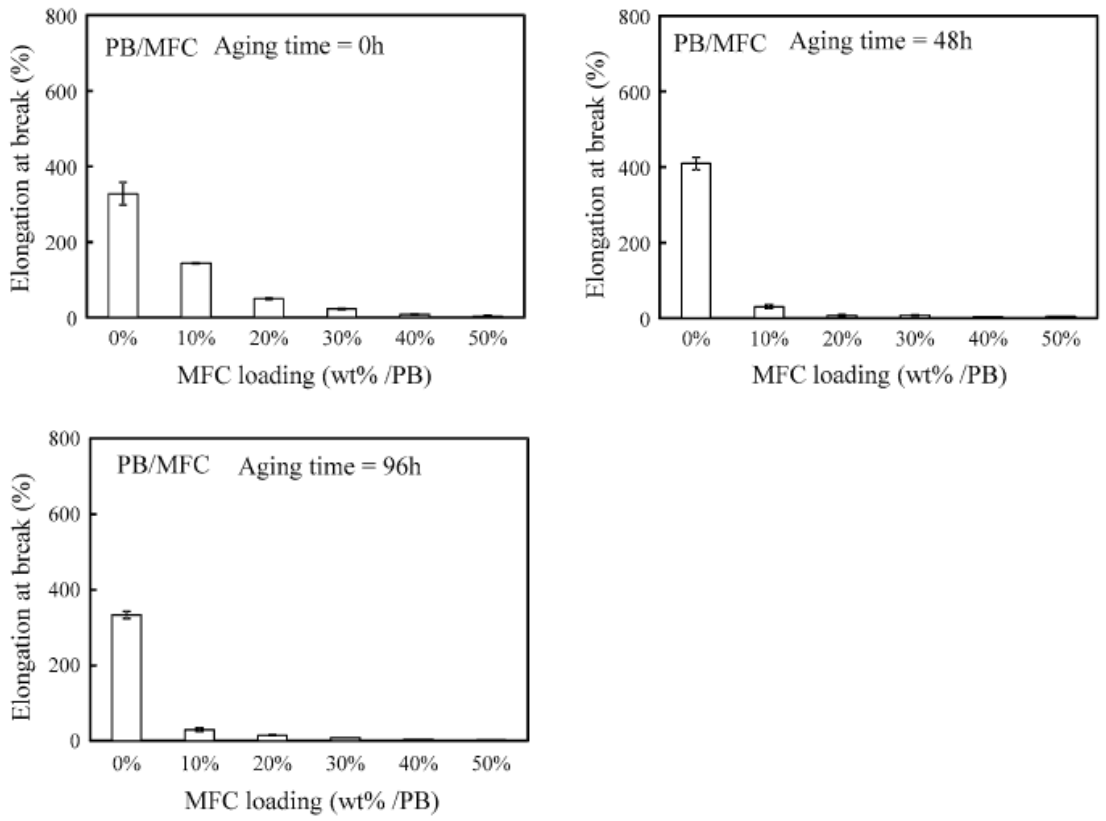

Fig. 3 Comparison of elongation at break values of PB/MFC films and their aged ones. Aging temperature = r. t. (ca. 20℃)

loading without the aging treatment. The MFC (30 %) composite shows the slightly larger modulus although the error of the value is bigger. The moduli of the MFC (40 %) and MFC (50 %) are 74 and 73 % of those of the corresponding PB/MFC, respectively. It seems that the 10 % TP loading is too small to cover much amount of the MFC. These Young's moduli remarkably increase with the increase of aging time as well as those of the PB/MFC. Figure 6 shows the changes of I/II peak intensity ratio of various samples at r. t. (ca. 20℃). The I/II intensity ratio of the PB/MFC (10 %) is lower than that of the PB up the 72 h aging time, whereas, as a whole, that of the PB/TP (10 %) is higher. The results indicate that the MFC brocks the II–I crystal phase transformation during the initial aging, and the TP enhances the one. As shown in Fig. 6, the peak intensity ratio

of the PB/TP (10 %)/MFC (10 %) is distinctly higher than of the PB, showing the TP enhancement effect strongly appears. The behavior shows that the interface between the PB and MFC is certainly composed of TP component, supporting that the TP works as the good compatibilizer. In addition, the I/II intensity ratio of the PB/TP (10 %)/MFC (10 %) is considerably higher than that of the PB/TP (10 %) during all of the aging time. The behavior suggests that the TP in the PB/TP (10 %)/ MFC (10 %) is well dispersed due to its attaching to the MFC. As shown in Fig. 7, the elongation at break values of the PB/TP (10 %)/MFC are 99–281 % of those of the corresponding PB/MFC. The TP certainly works as plasticizer for PB [20].

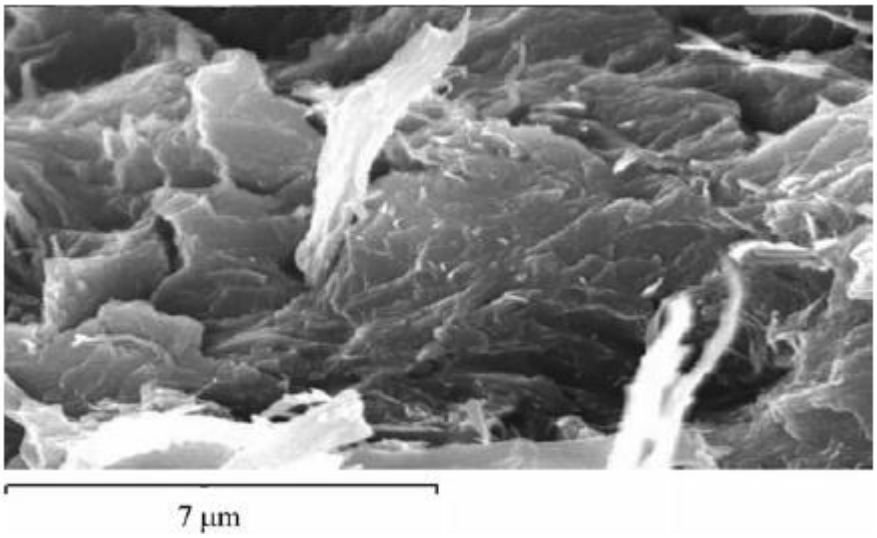

Fig. 4 SEM microphotograph of fractured surface of PB/TP (10 %)/MFC: TP content (wt%/PB), MFC loading = 10 wt%/PB

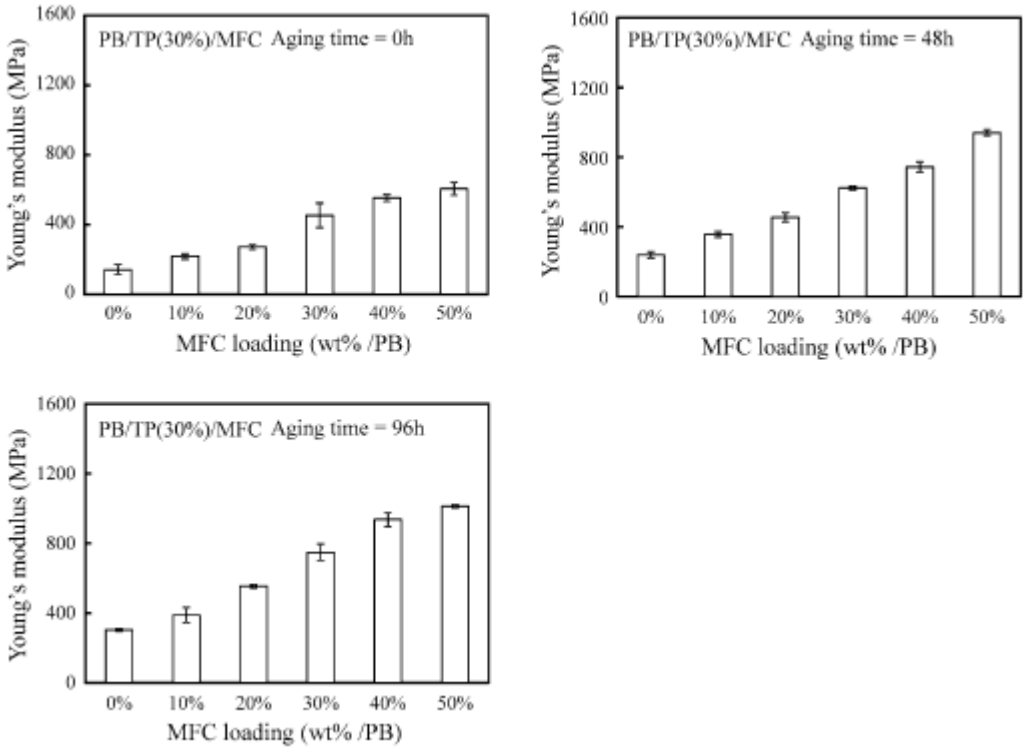

Fig. 5 Comparison of Young's moduli of PB/TP (10 %)/MFC films and their aged ones. TP content (wt%/PB). Aging temperature = r. t. (ca. 20 ℃)

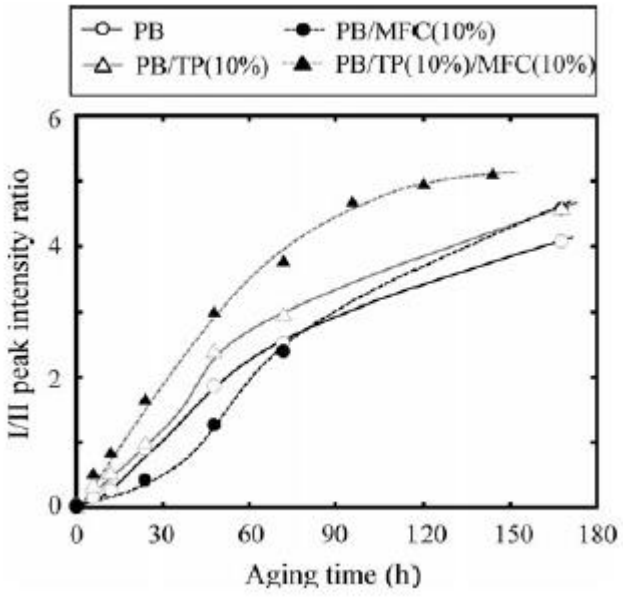

Fig. 6 Changes of I/II peak intensity ratio of various samples at r. t. (ca. 20 ℃). TP and MFC contents (wt%/PB)

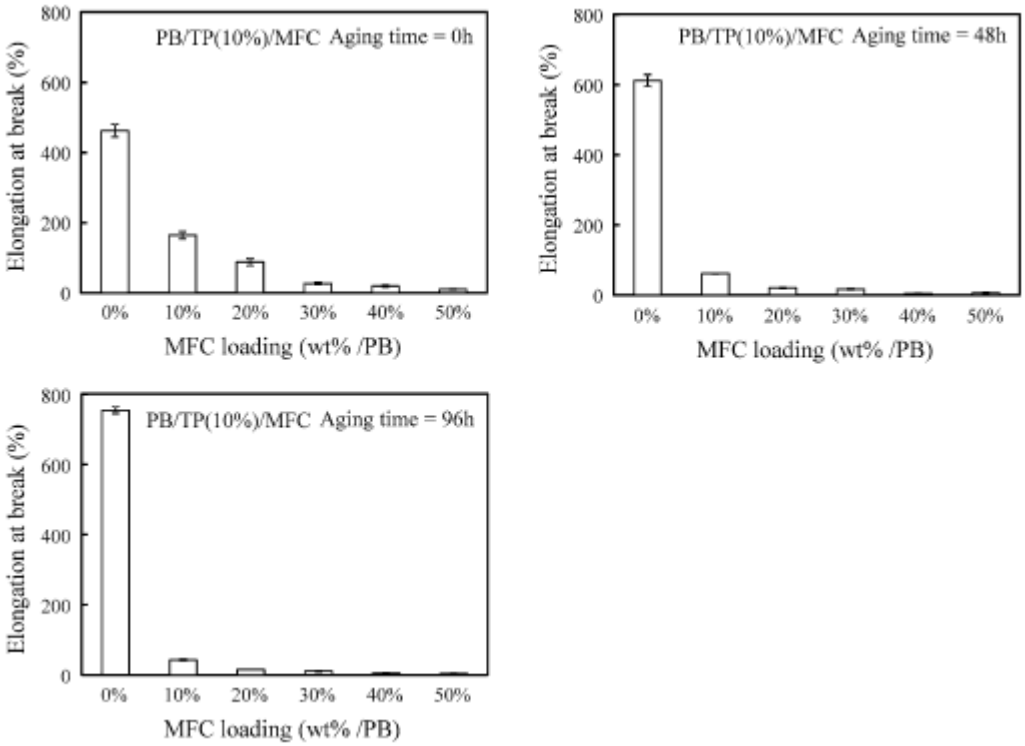

Fig. 7 Comparison of elongation at break values of PB/TP (10 %)/MFC films and their aged ones. TP content (wt%/PB). Aging temperature = r. t. (ca. 20 ℃)

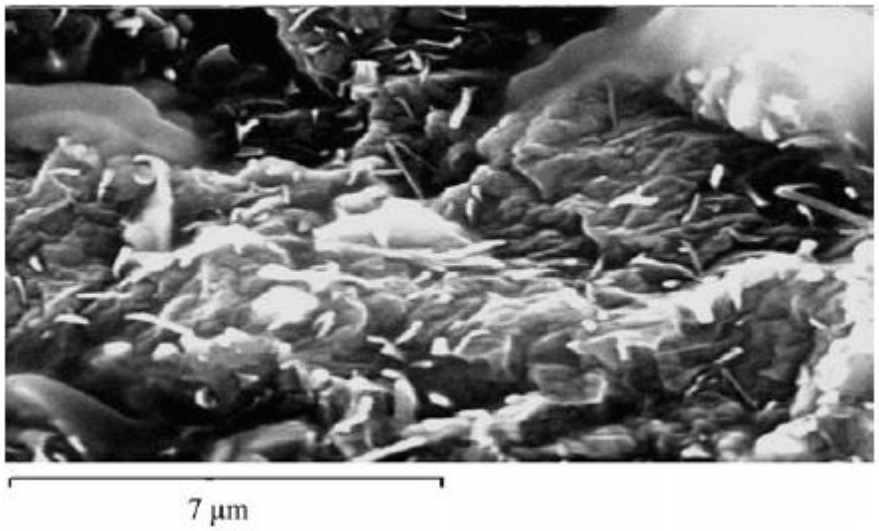

Fig. 8 SEM microphotograph of fractured surface of PB/TP (30 %)/MFC: TP content (wt%/PB), MFC loading = 10 wt%/PB

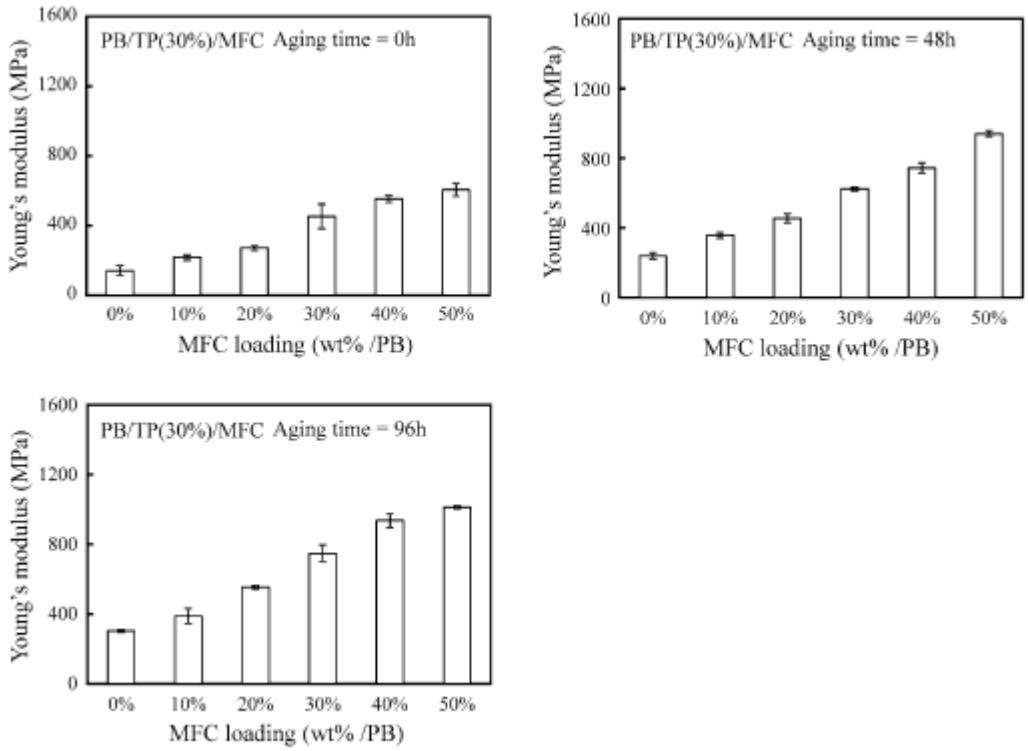

Fig. 9 Comparison of Young's moduli of PB/TP (30 %)/MFC films and their aged ones. TP content (wt%/PB). Aging temperature = r. t. (ca. 20 ℃)

Figure 8 shows the SEM microphotograph of fractured surface of the PB/TP (30 %)/MFC (10 %). Many white MFC fibers can be observed. As compared with the MFC in the PB/TP (10 %)/MFC (10 %), the shape is defined and is thicker, suggesting that more TP attaches to the MFC. Figure 9 shows the Young's moduli of the PB/TP (30 %)/MFC with various MFC content and those of their aged ones. The moduli are 91–147 % of the corresponding PB/MFC without the aging treatment, and the aged those of MFC = 40 and 50 % content showed the slightly lower (73–93 %) moduli. In addition, as shown in Fig. 10, the elongation at break values of the PB/TP (30 %)/MFC are 38–94 % of those of the corresponding PB/TP (10 %)/MFC. The TP 30 % loading little improve the tensile properties of PB/MFC as compared with the 10 % loading.

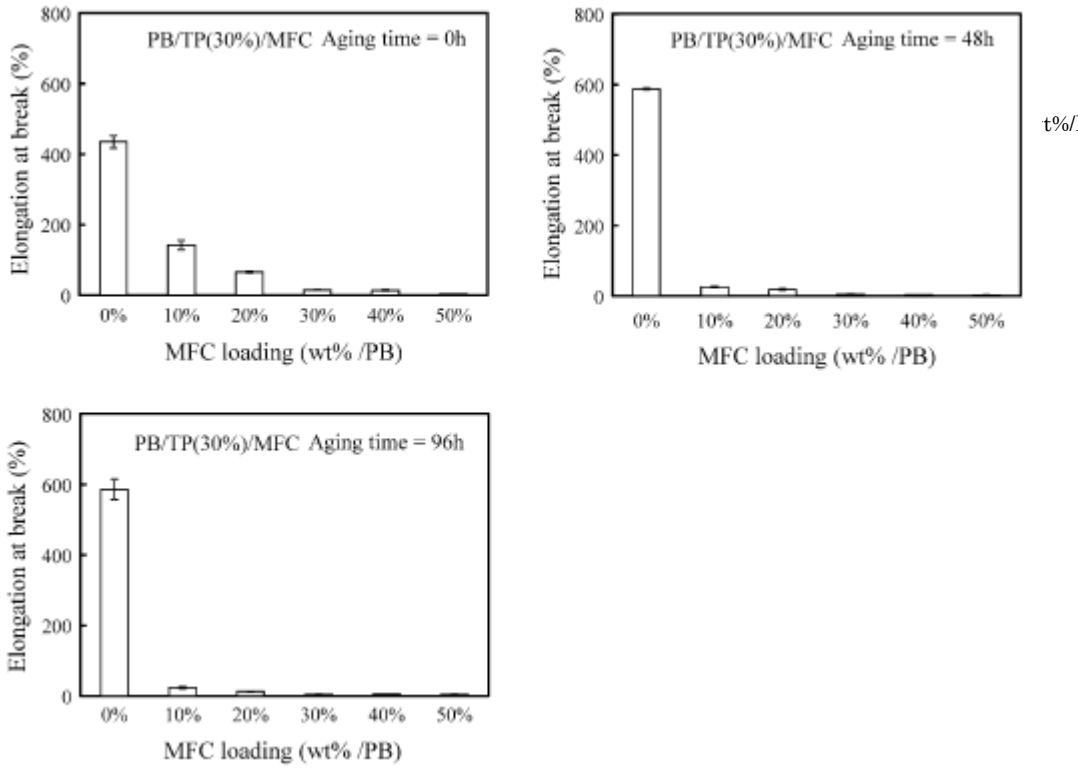

t%/PB). Aging

Fig. 10 Comparison of elongation at break values of PB/TP (30 %)/MFC films and their aged ones. TP content (wt%/PB). Aging temperature = r. t. (ca. 20℃)

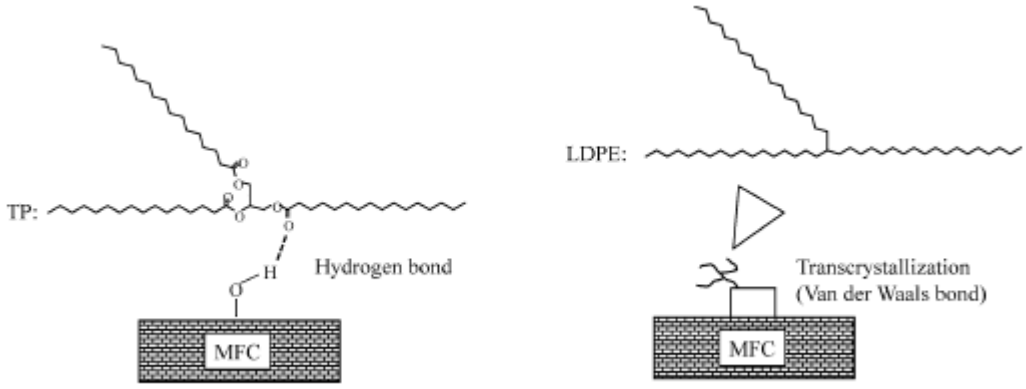

Fig. 11 Interface structures of TP/MFC and LDPE/MFC

The TP loading brings about the good dispersibility of MFC and works plasticizer for PB. However, the TP interface strength is poor due to low molecule. It seems that polymeric interface is favorable for enhancement of the tensile properties such as

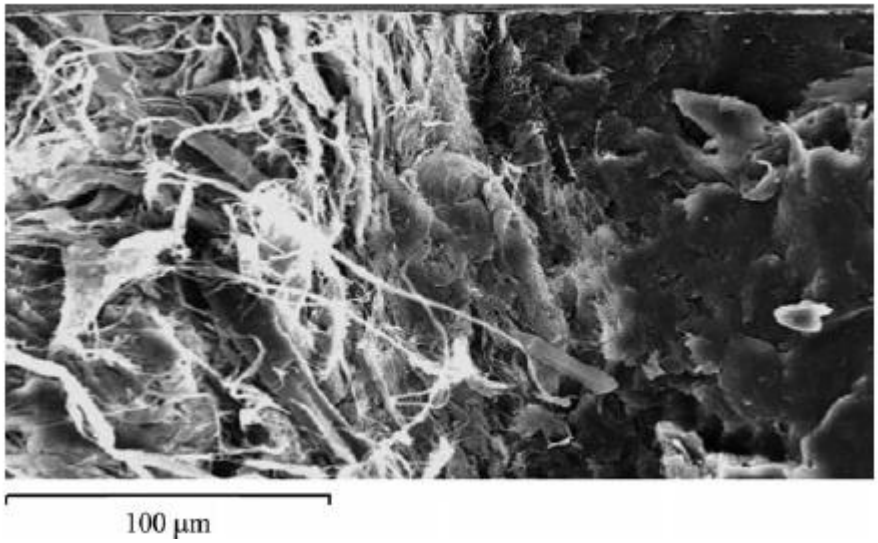

Fig. 12 SEM microphotograph of fractured surface of PB/LDPE (10 %)/MFC: LDPE content (wt%/PB), MFC loading = 10 wt%/PB

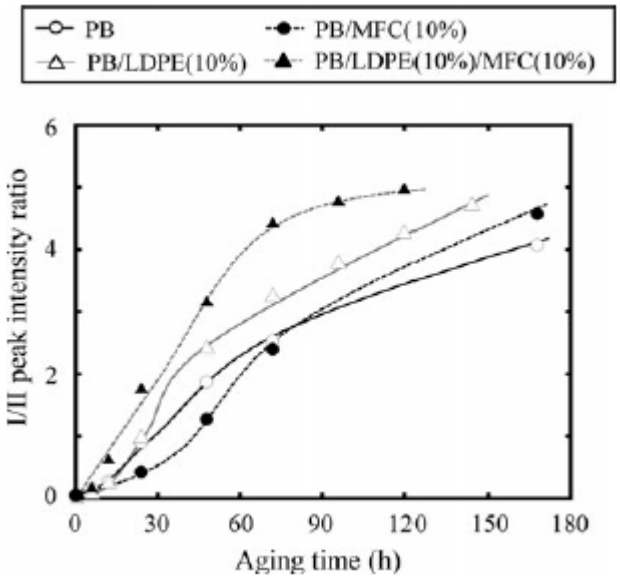

Fig. 13 Changes of I/II peak intensity ratio of various samples at r. t. (ca. 20 ℃). LDPE and MFC contents (wt%/ PB)

Young's modulus. LDPE and PB polymer blend has been commercially used for peel film packages although it shows thermodynamic immiscibility [23]. It seems that the interface between LDPE and PB has a certain level of adhesive strength due to unique nature of LDPE crystal orientation [23]. The LDPE loading has a potential to improve the tensile properties of the PB/MFC composite. Figure 11 shows the interface

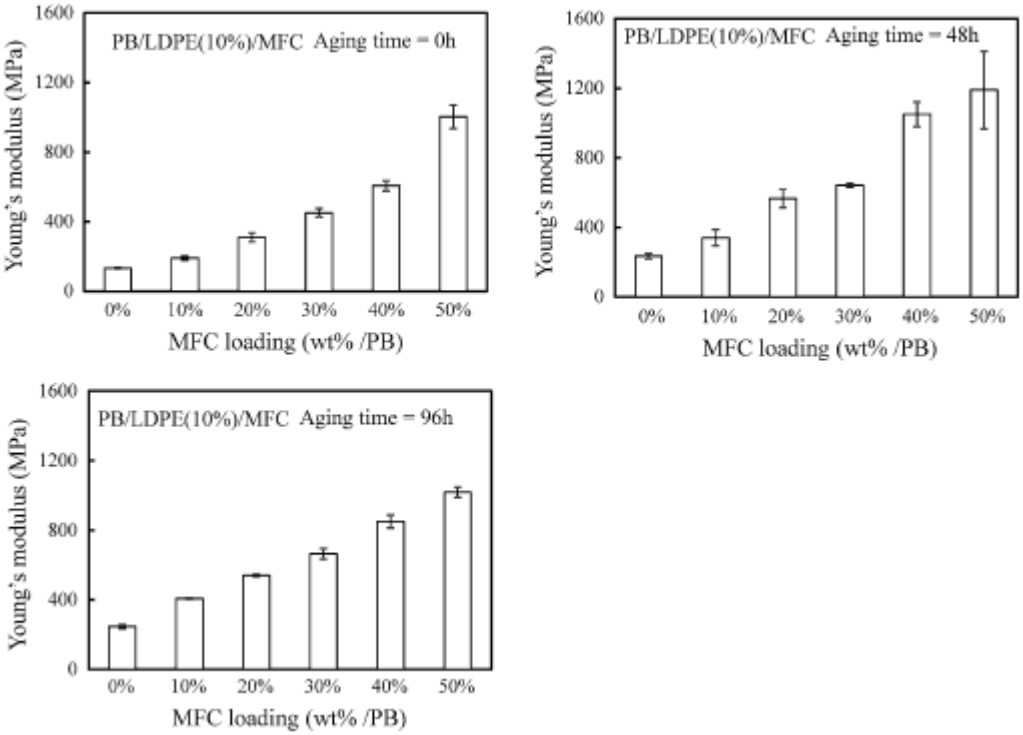

Fig. 14 Comparison of Young's moduli of PB/LDPE (10 %)/MFC films and their aged ones. TP content (wt%/PB). Aging temperature = r. t. (ca. 20 ℃)

structures of TP/MFC and LDPE/MFC. LDPE molecular structure is similar to TP one, however, it does not contain ester group. As shown in Fig. 11, the TP chain can attach to MFC surface with hydrogen bond. The LDPE chain attachment has no choice but to use Van der Waals bond and leads to the transcrystallization due to its high crystallization nature. The LDPE transcrystal grows, and the MFC surface is covered with spines of the transcrystal. It seems that the interface strength between the PB and MFC is physically improved by the existence of the LDPE spine. As shown in Fig. 12, the SEM microphotograph of fractured surface of the PB/LDPE (10 %)/MFC (10 %) shows the MFC entanglement as well as that of the PB/MFC (10 %). Although large aggregation of the MFC hardly occurs, the dispersity in the PB matrix is considerably poor as compared with that of the PB/TP (10 %)/MFC (10 %). Figure 13 shows the changes

of I/II peak intensity ratio of various samples. The I/II intensity ratio of the PB/LDPE (10 %) is higher than that of the PB, and that of the PB/LDPE (10 %)/MFC (10 %) is much higher. The behavior is the same as the PB/TP (10 %) and PB/TP (10 %)/MFC (10 %), suggesting that the LDPE exists in the interface between the PB and MFC. Figure 14 shows the Young's moduli the of PB/LDPE (10 %)/MFC with various MFC content and those of their aged ones. The moduli are 5–51 % higher than those of the corresponding PB/MFC without the aging treatment. The modulus of the MFC (50 %) loading is reached up to ca. 1 GPa, and its value is 151 % of that of the PB/MFC (50 %). The moduli of the PB/TP (10 %)/MFC (50 %) and PB/TP (30 %)/MFC (50 %) are 485 and 606 GPa, respectively and are considerably lower. The superiority is certainly kept up to the 48 h aging treatment and is lost at the 98 h one. The phase separation between PB and LDPE is developed by the II–I crystal phase transformation, and the interface strength becomes week. Figure 15 shows the elongation at break values of the PB/LDPE (10 %)/MFC films and their aged ones. The values of the PB/LDPE (10 %)/MFC are 48–139 % of those of the corresponding PB/MFC. The improvement effect of the LDPE loading on the elongation at break value is considerably less than that of the TP loading. The composite rapidly becomes embrittlement by the higher MFC content and aging.

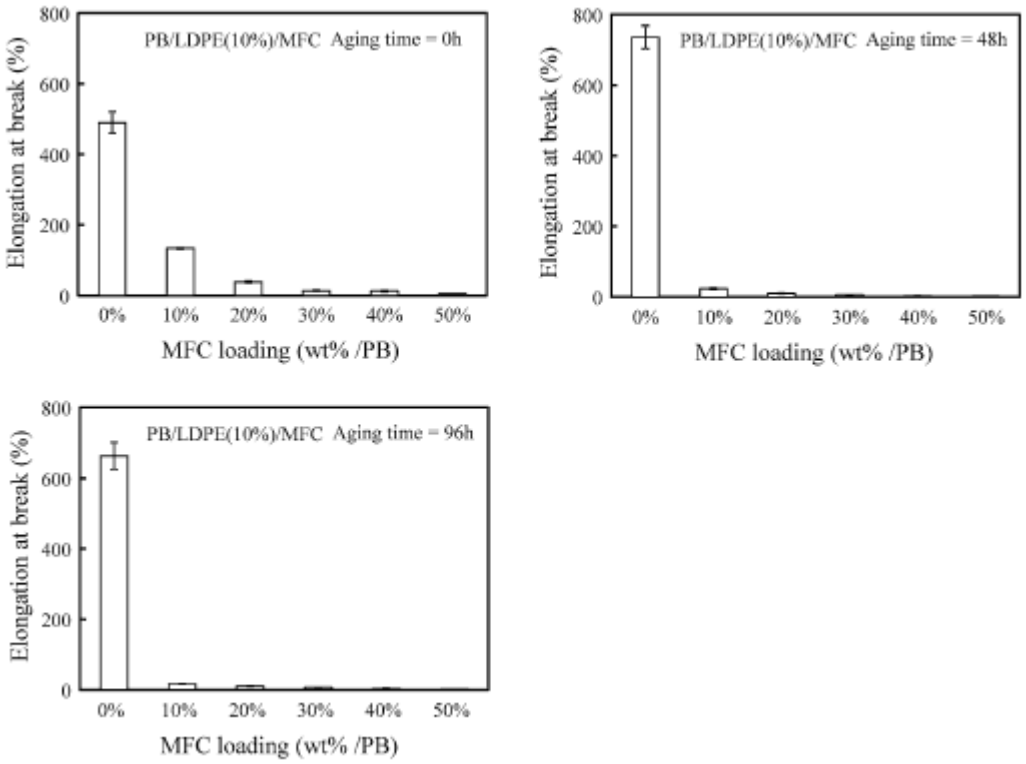

Fig. 15 Comparison of elongation at break of PB/LDPE (10 %)/MFC films and their aged ones. TP content (wt%/PB). Aging temperature = r. t. (ca. 20 ℃)

4-4 Conclusions

In this work, the effects of the TP and LDPE loadings on the tensile properties of PB/MFC composite were studied. The TP loading brought about good dispersity of the MFC in PB matrix. The Young's modulus and elongation at break values of the composite are slightly decreased and are considerably increased by the TP 10 % loading. The TP 30 % loading little improved the tensile properties of the composite as compared with the 10 % loading. The TP loading was of limited effectiveness for the improvement of the tensile properties, suggesting that polymeric interface was suitable for enhancement of the tensile properties such as Young's modulus. In fact, the LDPE 10 % loading brought about the large increment of the Young's modulus for the composite although the improvement effect on the elongation at break value was less than that of the TP loading.

References

1. W. Qiu, F. Zhang, T. Endo, T. Hirotsu, (Milling-induced esterification between cellulose and maleated polypropylene)., *J. Appl. Polym. Sci.* **2004,** 91, 1703–1709.

2. J. M. Felix, P. Gatenholm, (The nature of adhesion in composites of modified cellulose fibers and polypropylene)., *J. Appl. Polym. Sci.* **1991,** 42, 609–620.

3. W. Qiu , T. Endo, T. Hirotsu, (Interfacial interactions of a novel mechanochemical composite of cellulose with maleated polypropylene)., *J. Appl. Polym. Sci.* **2004,** 94, 1326–1335.

4. V. N. Hristov, S. T. Vasileva, M. Krumova, R. Lach, G. H. Michler, (Deformation mechanisms and mechanical properties of modified polypropylene/wood fiber composites)., *Polym Compos.* **2004,** 25, 521–526.

5. K. Miyazaki, K. Moriya, N. Okazaki, M. Terano, H. Nakatani (Cellulose/polypropylene composites: influence of the molecular weight and concentration of oxidatively degraded and maleated polypropylene compatibilizers on tensile behavior),. *J. Appl. Polym. Sci.* **2009,** 111, 1835–1841.

6. H. Nakatani, K. Miyazaki, (Modification of polypropylene and polypropylene/fibrous cellulose composites by the addition of polyethylene oxide). J. Appl. Polym. Sci. **2009,** 112, 3362–3370.

7. H. Nakatani, K. Hashimoto, K. Miyazaki, M. Terano, (Cellulose/syndiotactic polypropylene composites: effects of maleated polypropylene as a compatibilizer and silanized cellulose on the morphology and tensile properties)., *J. Appl. Polym. Sci.* **2009,** 113, 2022–2029.

8. K. A. Afrifah, R. A. Hickok, L. M. Matuana, (Polybutene as a matrix for wood plastic composites)., *Compos Sci Technol.* **2010,** 70, 167–172.

9. A. T. Jones, (Cocrystallization in copolymers of a-olefins II—Butene-1 copolymers and polybutene type II/I crystal phase transition)., *Polymer.* **1966,** 7, 23–59.

10. K. W. Chau, Y. C. Yang, P. H. Geil, (Tetragonal twinned hexagonal crystal phase transformation in polybutene-1)., *J. Mater. Sci.* **1986,** 21, 3002–3014.

11. Y. T. Shieth, M. S. Lee, S. A. Chen, (Crystallization behavior, crystal transformation, and morphology of polypropylene/polybutene-1 blends),. *Polymer.* **2001,** 42, 4439–4448.

12. G. C. Alfonso, F. Azzurri, M. Castellano, (Analysis of calorimetric curves detected during the polymorphic transformation of isotactic polybutene-1),. *J. Therm. Anal. Calorim.* **2001,** 66, 197–207.

13. F. Azzurri, A. Flores, G. C. Alfonso, I. Sics, B. S. Hsiao, F. J. B. Calleja, (Polymorphism of isotactic polybutene-1 as revealed by microindentation hardness. Part II: correlations to microstructure),. *Polymer.* **2003,** 44, 1641–1645

14. R. Hadal, Q. Yuana, J. P. Jog,R. D. K. Misra, (On stress whitening during surface deformation in clay-containing polymer nanocomposites: a microstructural approach),. *Mater Sci Eng*, **2006,** A 418, 268–281.

15. M. Nase, R. Androsch, B. Langer, H. J. Baumann, W. Grellmann, (Effect of polymorphism of isotactic polybutene-1 on peel behavior of polyethylene/polybutene-1 peel systems)., *J. Appl. Polym. Sci.* **2008,** 107, 3111–3118.

16. H. Nakatani, Y. Yamada, Y. Takahashi, M. Terano, (Effects of crystal phase transformation on tensile properties of polybutene-1/cellulose composites),. *J. Appl. Polym. Sci.* **2012**, 123:41–49.

17. E. Weynant, J. M. Haudin, C. G'Sell, (Plastic deformation and solid-phase transformation in polybutene-1),. *J. Mater. Sci.* **1982,** 17, 1017–1035.

18. H. Nakatani, T. Ichizyu, H. Miura, M. Terano, (Novel modification of polybut-1-ene using autooxidation controlled by addition of limonene monomer),. *Polym Int.* **2010,** 59, 463–471.

19. H. Nakatani, T. Ichizyu, H. Miura, M. Terano, (You have full text access to this contentPreparation of modified polybutene-1 by oxidation and limonene radical grafting using an Nd2O3-assisted radical initiator system and its characterization),. *Polym Int* **2010,** 59, 1673–1682.

20. K. Miyazaki, Y. Takahashi, M. Terano, H. Nakatani, (Additive effects of tripalmitin on morphologies and tensile properties of polybutene-1 and its composite with micro fibrous cellulose),. *Polym Bull.* **2013,** 70, 1383–1395.

21. J. H. Moffitt, B. A. Fielding, R. Evershed, R. Berstan, J. M, Currie, A.Clark, (Adverse physicochemical properties of tripalmitin in beta cells lead to morphological changes and lipotoxicity in vitro),. *Diabetes* **2005,** 48, 1819–1829.

22. P. Fairley, J. M. KKrochta, I. B. German, (Crystal morphology of mixtures of tripalmitin and butterfat)., *J. Am. Oil. Chem. Soc.* **1995,** 72, 693–697.

23. M. Nase, S. S. Funari, G. H. Michler, B. Langer, W. Grellmann, R. Androsch, (Structure of blown films of polyethylene/polybutene-1 blends)., *Polym. Eng. Sci.* **2010,** 50, 249–256.

24. H. Nakatani, Y. Yamada, Y. Takahashi , M. Terano, (Effects of crystal phase transformation on tensile properties of polybutene-1/cellulose composites)., *J. Appl. Polym. Sci.* **2011,** 123, 41–49.

Chapter5

Effect of Polymer Chain Scission on Photodegradation Behavior of Polystyrene/Multi-Wall Carbon Nanotube Composite

5-1: Introduction

Carbon nanotube (CNT) is one of the attractive filler materials for polymer composite from the viewpoints of good electrical,[1] mechanical,[2,3] and thermal4 properties. CNT is a long filler, resulting that the entanglement occurs. The entanglement brings about a three-dimensional network structure (percolation) of CNT.[5] Formation of the percolation in the polymer composite brings about considerable improvement in the electrical conductivity even with a small amount of the loading.[6–9] For instance, in the case of polyepoxy matrix, the percolation threshold was reported to be ca. 0.0025 wt % CNT loading.[6] The high aspect ratio allows other properties to be strongly improved by even a small loading as well.[9–11] Great efforts simultaneously have been made on oxidative degradation of CNT/polymer composites from the point of view of an improvement to the resistance.[12– 17] However, it seems that the improvement has been not well developed by a small loading.[12–14]

Auto-oxidation is one of oxidative degradation and a majordegradation mechanism in polymeric materials.[18–22] There is much literature on the mechanism. Many researchers agree fundamentally with the following mechanistic scheme:

$$\text{Initiation} : RH \rightarrow R\bullet \quad (1)$$

$$\text{Propagation} : R\bullet + O_2 \rightarrow ROO\bullet \quad (2)$$

$$ROO\bullet + RH \rightarrow R\bullet + ROOH \quad (3)$$

Chain branching (including chain scission)

$$ROOH \rightarrow \text{carbonyls} + R\bullet \quad (4)$$

The auto-oxidation is mainly composed of the radical reactions. It is assumed that CNT works as a polymer antioxidant since it has an ability to scavenge radical species with

graphene structure. In fact, however, the antioxidant effect was quite small for the composite,[12–14] and on the contrary, the CNT worked as pro-oxidant at a low loading amount.[12,14] Several scientists proposed that the pro-oxidant effect was most likely due to the local increase of the temperature induced by CNTs.[13,14] They concluded that the antagonism between the antioxidant and pro-oxidant effects produced either the stabilizing or prodegradant one. We have considered that there exists another factor working as the pro-oxidant. Well-dispersion of multi-wall carbon nanotube (MWNT) frequently requires a severe dispersion treatment such as high speed mixing and combination of sonicated and stirred methods,[23–25] resulting that scission of the polymer chain certainly occurs. In fact, P€otschke et al. reported that there was a decrease in molecular weight of all extruded poly(caprolactone) (PCL)/MWNT composites as compared to unprocessed virgin PCL.[26] The chain scission certainly produces unsaturated and carbonyl groups working as pro-oxidant for the polymer degradation. It seems that the chain scission considerably affects the degradation behavior. However, the effect has been not studied yet.

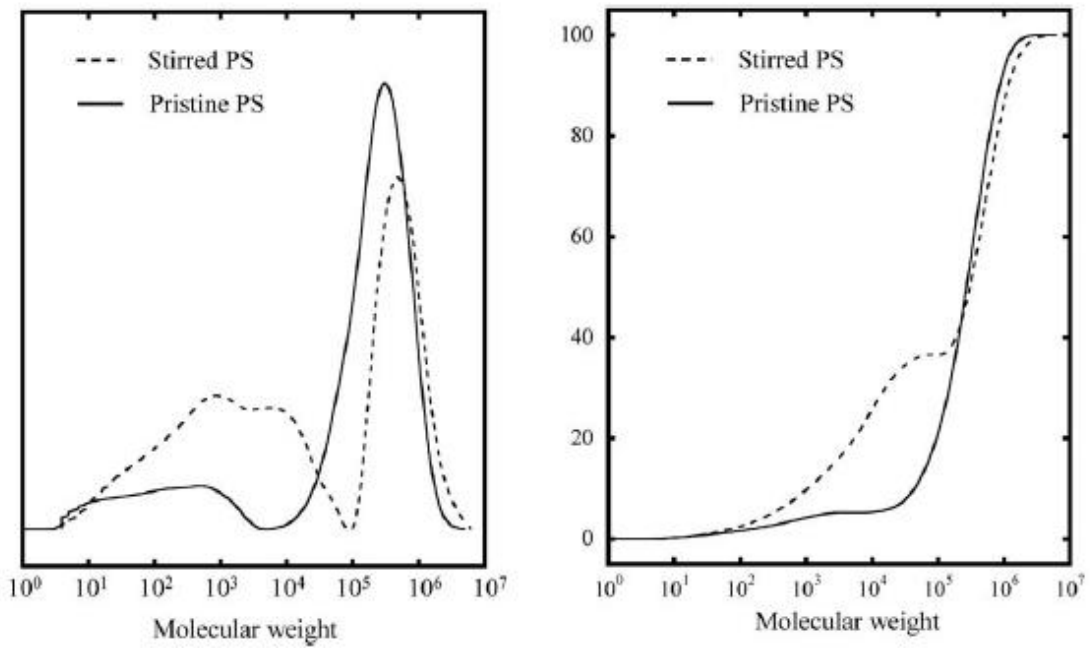

Fig. 1 Differential and integral molecular weight distribution curves of pristine and stirred PS samples.

In order to clarify the effect of the chain scission on the polymer degradation, polystyrene (PS)/MWNT composite was employed, and a relationship between the change of molecular weight and photodegradation behavior was studied. In addition, the antioxidant activity of the MWNT in the PS composite was evaluated using electrical conductivity and molecular weight measurements.

5-2: Experimental

5-2-1: Raw Materials

PS was purchased from Sigma-Aldrich Co. LLC. The gel permeation chromatography (GPC) curve was composed of two peaks. The weight-average molecular weight (M_w) and molecular weight distribution (M_w/M_n) of the major and minor peaks were 3.6×10^5 and 1.3×10^3, 3.0, and 1.2, respectively. MWNT was synthesized through dissociation of methane at 750℃ with a Fe_2O_3 catalyst. The diameter was from about 20 nm to 80 nm,

and the length was from 0.1 μm to 3 μm. The MWNT was well purified and almost no catalyst was on it to influence the PS degradation behavior. Tetrahydrofuran (THF) was purchased from Wako Pure Chemical Industries, Ltd.

5-2-2: Preparation of PS/MWNT Composite Film

The PS/MWNT composite film was prepared by solvent-casting method. The mixture of PS and MWNT was vigorously stirred with a magnetic stirrer at 300 rpm in 10 wt % THF solution, and then the solvent was allowed to evaporate for 12 h. The cast film was further dried under vacuum at room temperature for 8 h. The thickness was kept at about 600 μm.

5-2-3: Photodegradation Condition

The film was laid on a petri dish. A mercury vapor lamp of 400W (Toshiba H-400P, luminance value = 200 cd/cm^2) was used as a UV light source. The distance between specimens and the lamp was 50 cm. The photodegradation tests were carried out at 30℃.

5-2-4: Gel Permeation Chromatography Analysis

Sample in a small vial was dissolved in 5 mL of chloroform, and the sample solution was directly measured by GPC. The molecular weight was determined by GPC (SHIMADZU, Prominence GPC system) at 40℃ using chloroform as a solvent.

5-2-5: Electrical Conductivity Measurement

The electrical conductivity of the film samples with about 600 μm thickness was

determined at room temperature by a conventional four-point-probe technique with a resistivity meter (Loresta-GP MCP-T610, Mitsubishi Chemical Co.).

5-2-6: Fourier Transform Infrared Analysis

The Fourier transform infrared (FTIR) spectrum (one scan) of the film sample surface was recorded on a JASCO FT/IR-660 plus spectrometer with ATR PRO450-S accessory and ZnSe. Carbonyl index was obtained from carbonyl (at 1713 cm^{-1}) and aromatic ring breathing (at 1452 cm^{-1}) peak absorbance ratio (A_{1713} cm^{-1}/A_{1452} cm^{-1}).

5-3: Results and discussion

Figure 1 shows the differential and integral molecular weight distribution curves of the pristine and stirred PS samples. The differential curve of the stirred PS shows a drastic increase of the peak intensity in the low molecular weight (less that 10^5) region as compared with that of the pristine one. In addition, the main peak slightly shifts to a higher molecular weight. The integral molecular weight distribution curves show that the less than 10^5 and over 10^6 fractions in the pristine and stirred PS samples are 27.4 and 37.1%, and 8.6 and 15.7%, respectively. When the PS is stirred with a magnetic stirrer at 300 rpm, the polymer chain scission is certainly caused by the shear stress. As shown in Scheme 1, the PS chain is mechanically broken by the shear stress and produces a PS radical species. The radical species disproportionates and produces the PS chain with an unsaturated end group. The unsaturated end group has a potential to become a degradation initiating site leading to autooxidation and crosslink reactions.[27,28] In fact, the main peak of the stirred PS slightly shifts to the higher

molecular weight, indicating that a crosslink reaction occurs.

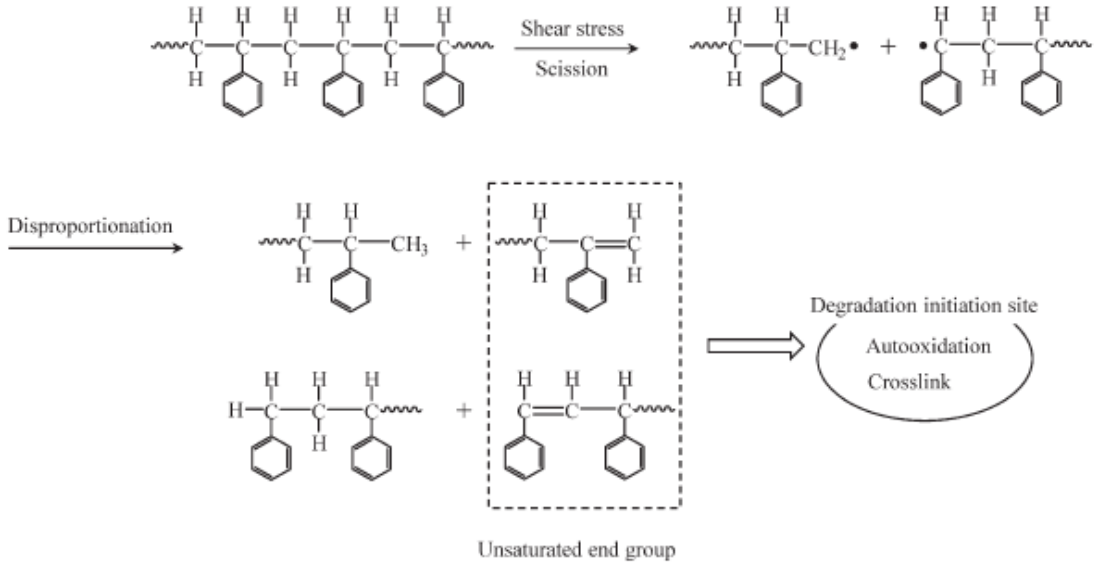

Scheme 1. Production process of degradation initiate site by shear stress

Well-dispersion of MWNT frequently requires a severe dispersion treatment such as high speed mixing and combination of sonicated and stirred methods.[23–25] In addition, MWNT is much rigid, and its loading certainly brings about severe polymer chain scission. Figure 2 shows the molecular weight curves and less than 10^5 molecular weight fractions of PS/MWNT composites. As shown in the differential molecular weight distribution curves, the MWNT loading certainly leads to the increase of the peak intensity in the low molecular weight (less than 10^5) region. However, the increase of the less than 10^5 molecular weight fraction is not proportional to the loading amount. The fraction value changes from 44% to 58% between the 1% and 4% MWNT content and shows the minimum one at 2%. The existence of the minimum value suggests that there exists other factor contributing to PS chain scission. When polymer chain encounters MWNT with high rigidity at high speed, it is surely cut. The encounter frequency definitely depends on rheology behavior of polymer/MWNT composite.

Guo et al. reported that during melt mixing, a long MWNT degraded polycarbonate

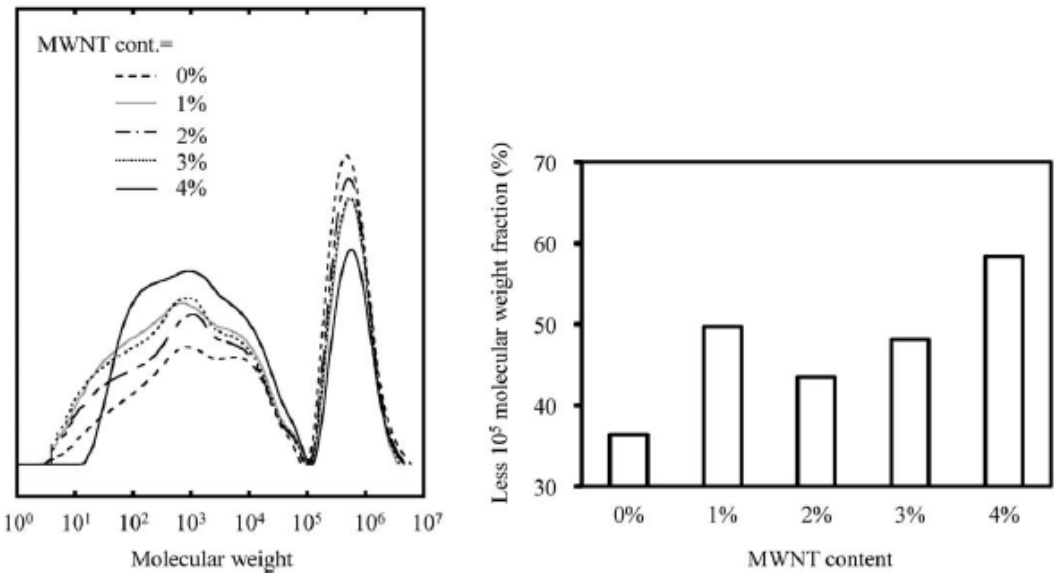

Figure 2. Differential molecular weight distribution curves and less than 105 molecular weight fractions of PS/MWNT composites.

polymer very much, but short ones barely did it.[17] The behavior indicates that there exists a rheological effect in polymer chain scission induced by MWNT loading. It seems that the peculiar behavior of the PS chain scission is due to such a rheological effect. Figure 3 shows the electrical conductivity of the PS/MWNT composite as a function of the MWNT loading amount. The entanglement brings about the CNT percolation,[5] leading to considerable improvement in the electrical conductivity even with a small amount of the loading.[6–9] When the electrical conductivity has a sizeable step of some orders of magnitude above a CNT weight fraction, the fraction value is called in particular "percolation threshold."[6–9] As shown in Figure 3, the PS/MWNT conductivity shows a drastic increase between the 1% and 2% of the MWNT content, indicating that the MWNT percolation structure is formed between them. It is considered that the percolation structure is basically completed at the 2% MWNT content. Figure 4 shows the change of MWNT aggregation structure as a function of the content. MWNTs are likely to become an aggregation due to some forces, i.e., the Van der Waals force. As

shown in Figure 4, it seems that the MWNT aggregate is regarded as uniform-size spherical particle at a low MWNT content such as 1%. When the content increases, the aggregates with various sizes are formed. The aggregate with a small size gets between the large ones, and then the percolation structure is completed.

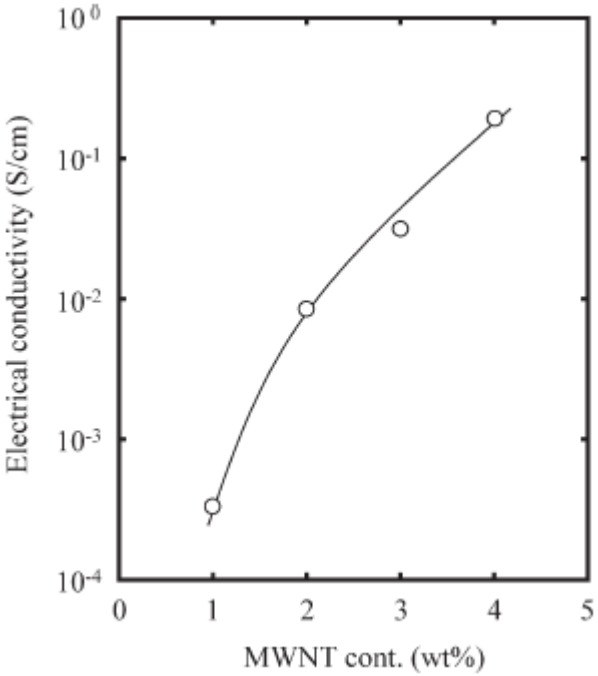

Figure 3. Electrical conductivity of PS/MWNT composite as a function of the MWNT loading amount.

Effects of particle size distributions on viscosities have been studied by Chong et al.[29] They reported that the fine particle acted like a ball bearing between large ones. The bearing effect brings about a decrease of viscosity, leading to the decrease of shear stress. It seems that the same effect occurs in the preparation of the PS/ MWNT composite. The small size MWNT aggregates act as ball bearings and lower the shear stress. The effect reaches a maximum at the 2% MWNT content, implying the decrease in number of the PS chain scission. The strange behavior showing the minimum fraction of the less than 105 molecular weight at the 2% MWNT content is due to such rheological effect.

The rheological effect makes the degradation behavior complex. Figure 5 shows the differential molecular weight distribution curves of un- and photodegraded PS and PS/MWNT samples. The PS curve shifts to a lower molecular weight by the 24-h photodegradation. The PS/MWNT curves do not show the behavior, and the main peak intensities become higher after the 24-h photodegradation. As shown in Figure 6, the

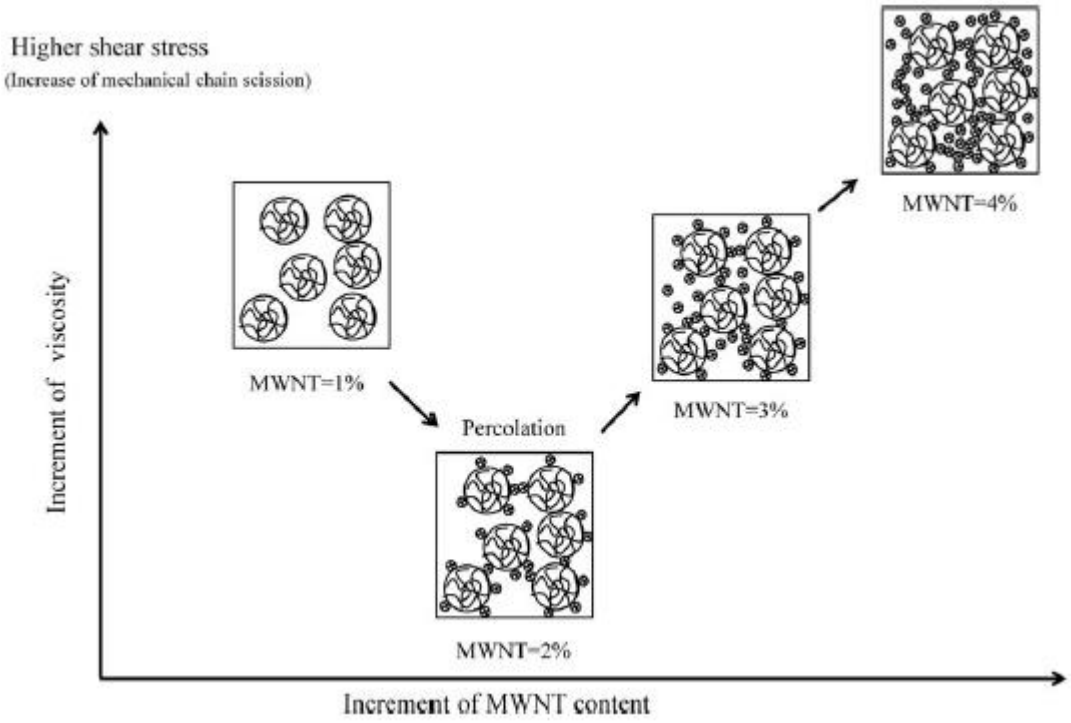

Figure 4. Change of MWNT aggregation structure as a function of the content.

less than 105 molecular weight fractions of the 24-h photodegraded PS/ MWNT samples decrease at 10.4%, 7.6%, 10.0%, and 15.1% in the 1%, 2%, 3%, and 4% MWNT content ones, respectively, although that of the 24-h photodegraded PS increases at 0.7%. The fraction decrease shows that the PS crosslink reaction occurs by the photodegradation. The crosslink reaction shows the maximum and minimum at the 4% and 2% MWNT content samples, respectively. Figure 7 shows the comparisons of carbonyl index (A_{1713} cm^{-1}/A_{1452} cm^{-1}) values of un- and photodegraded PS and PS/MWNT samples. The different values between the un- and photodegraded samples indicate degrees of the oxidative reaction (auto-oxidation) progress on the surfaces and are 0.246, 0.140, 0.017, 0.254, and 0.181 for the PS, 1%, 2%, 3% and 4% MWNT content samples, respectively. Although both the minimum values of the crosslink (the decrease of less than 10^5 molecular weight fraction) and oxidative (the different A_{1713} cm^{-1}/A_{1452} cm^{-1} value)

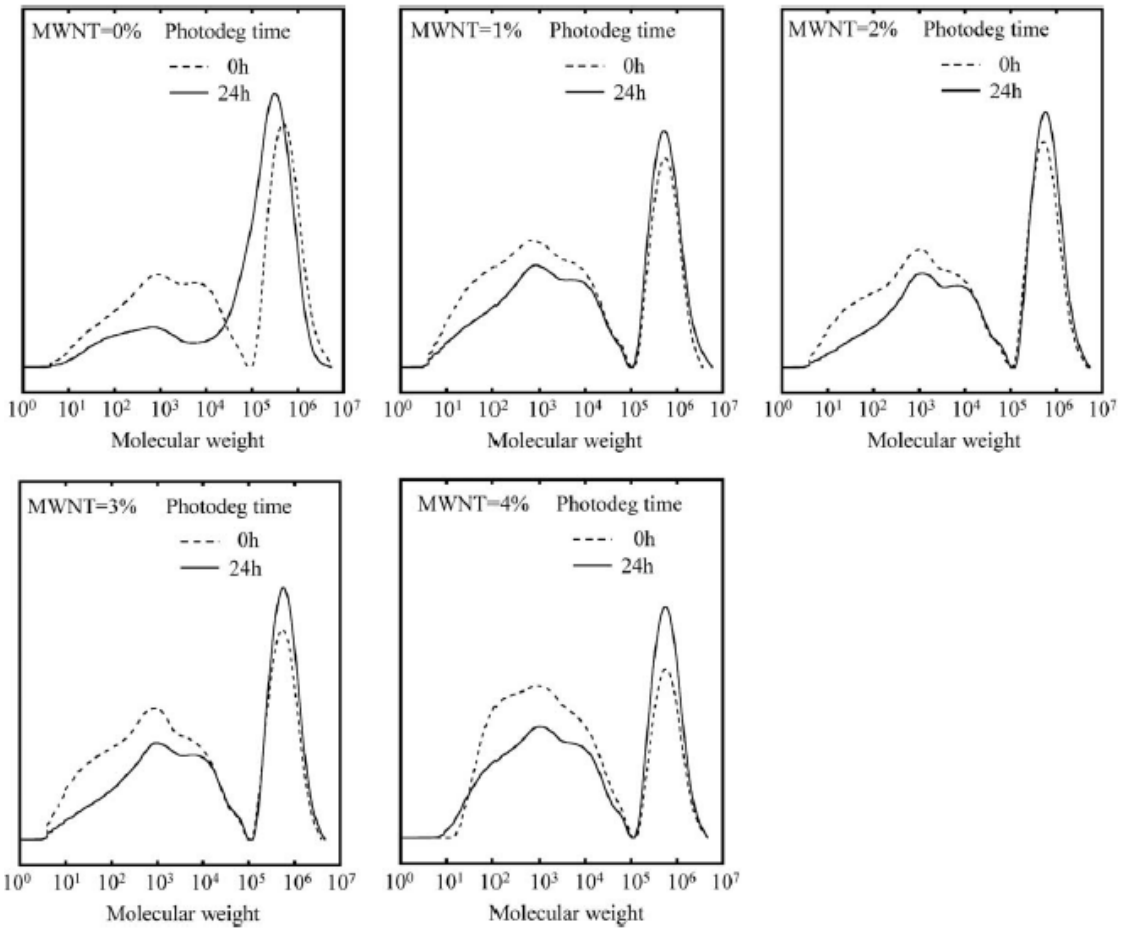

Figure 5. Differential molecular weight distribution curves of un- and photodegraded PS and PS/MWNT samples.

reactions are observed at the 2% MWNT content sample, the dependencies of both the values on the MWNT content do not agree well each other. As mentioned above, there exist the unsaturated end groups in these samples. The carbon double bonds and allyl protons next to them become crosslink points30 and initiation site of auto-oxidation,[25,26] respectively. Thus, the unsaturated end group certainly has a potential to become a degradation initiator leading to auto-oxidation and crosslink reactions. On the other hands, MWNT would have an ability to scavenge radical species and would work as antioxidant because of being composed of graphene structure with carbon double bond. The coexistence of the unsaturated end group and MWNT would lead to an antagonism in the degradation, making the behavior complicated.

However, the antioxidant effect of MWNT has been not clarified yet. Watts et al. reported that CNT worked as polymer antioxidants, and concurrently its effect was quite small for concentrations lower than 5%.[12] It seems that the ability of the MWNT radical scavenger is considerably low. It is necessary to evaluate the antioxidant ability. When the MWNT works as the radical scavenger, the electrical conductivity must be certainly lower due to a change of the graphene structure. The electrical conductivity degradation of the composite would be caused by a reaction with the generated radical species (i.e., radical reaction). The antioxidant activity of the MWNT in the PS composite can be evaluated by making a comparison between the conductivity and PS degradations. Figure 8 shows the

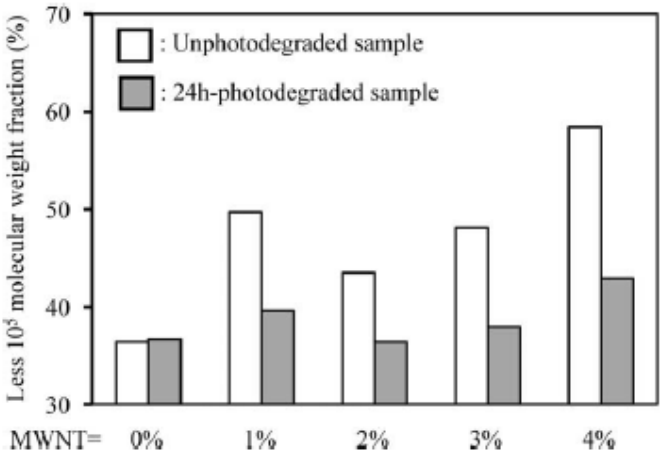

Figure 6. Less than 105 molecular weight fraction of un- and photodegraded

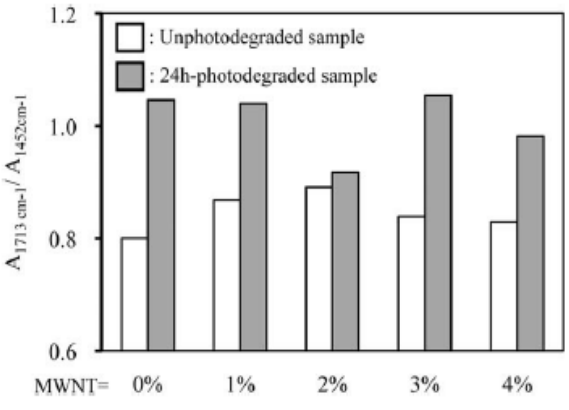

Figure 7. Comparisons of carbonyl index (A_{1713} cm^{-1}/A_{1452} cm^{-1}) values of un- and photodegraded PS and PS/MWNT samples: The FTIR measurement was carried out with FTIR spectrometer with ATR accessory

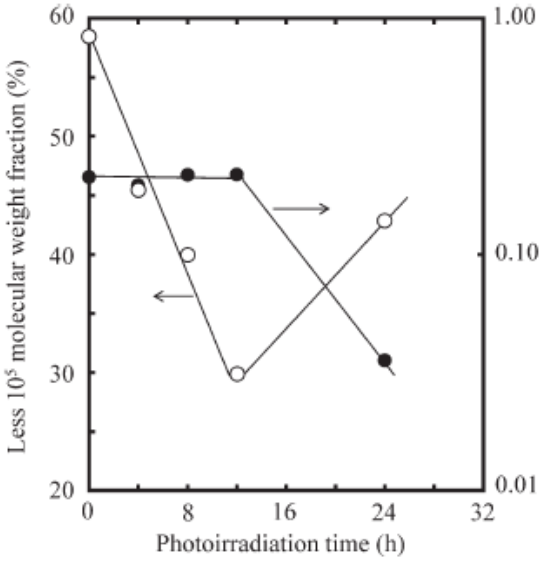

Figure 8. Changes of less than 10^5 molecular weight fraction and of electrical conductivity as a function of photodegradation time.

changes of less than 10^5 molecular weight fraction and of electrical conductivity as a function of photo-irradiation time. The electrical conductivity is almost constant up to the 12-h photoirradiation time and then drastically decreases at the 24 h one. On the other hands, the less than 105 molecular weight fraction drastically decreases up to the 12 h and increases at the 24 h. The value shows the ups and downs for the irradiation time. Such oscillating behavior is due to competition reaction between the PS chain scission and crosslinking and is typical of PS photodegradation. [30] The PS degradation is considerably sensitive to the initial photo-irradiation. The electrical conductivity degradation is not initially observed and is much insensitive to it. The MWNT radical scavenging ability is considerably poor although MWNT certainly works as the radical scavenger. MWNT is a filler material and is unable to molecularly disperse in polymeric matrix. The poor dispersity lowers the radical scavenging ability as compared with common antioxidant such as phenol and hindered amine light stabilizers. The antioxidant effect of MWNT is poor, and MWNT has little ability to inhibit the degradation initiation of the polymeric matrix.

5-4: Conclusions

In order to clarify the effect of the chain scission on the polymer degradation, the PS/MWNT composite was employed, and the relationship between the change of molecular weight and photodegradation behavior was studied. The MWNT loading brought about severe PS chain scission, leading to the increase of the low molecular weight (less than 10^5) fraction. The increase was not proportional to the loading amount and showed the minimum at the 2% loading. The behavior was due to a bearing effect

bringing about the decrease of shear stress. The unsaturated end group was produced by the chain scission and became the photodegradation initiator, leading to autooxidation and crosslink reactions. The MWNT scavenged radical species and worked as antioxidant. The coexistence of the unsaturated end group and MWNT made the photodegradation behavior complicated. However, the MWNT radical scavenging ability was considerably poor, and the MWNT had little ability to inhibit the photodegradation initiation.

References

1. C. A. Grimes, E. C. Dickey, C. Mungle, K. G. Ong, D. Qian, *J. Appl. Phys.* **2001**, 90, 4134.

2. O. Lourie, D. M. Cox, Wagner. H. D. *Phys. Rev. Lett.* **1998**, 81, 1638.

3. M.-F. Yu, B. S. Files, S. Arepalli, S. Ruoff, R. S. *Phys. Rev. Lett.* **2000**, 84, 5552.

4. S, Berber, Y-K Kwon, Tom_anek, D. *Phys. Rev. Lett.* **2000**, 84, 4613.

5. P. P€otschke, A. R. Bhattacharyya, A. Janke, Goering, H. *Compos. Interface.* **2003**, 10, 389.

6. J. K. W. Sandler, J. E. Kirk, I. A. Kinloch, M. S. P. Shaffer, Windle A. H. *Polymer.* **2003**, 44, 5893.

7. T. McNally, P. P€otschke, P. Halley, M. Murphy, D. Martin, S. E. J. Bell, G. P. Brennan, D. Bein, P. Lemoine, J. P. Quinn, *Polymer.* **2005**, 46, 8222.

8. G. Gorrasi, M. Sarno, A. D. Bartolomeo, D. Sannino, P. Ciambelli, Vittoria, V. J. *Polym. Sci. Part B: Polym. Phys*. **2007**, 45, 597.

9. O. Valentino, M. Sarno, N. G. Rainone, M. R. Nobile, P. Ciambelli, H. C. Neitzert, *G. P. Phys. E,* **2008**, 40, 2440.

10. D. Bikiaris, A. Vassiliou, K. Chrissafis, K. M. Paraskevopoulos, A. Jannakoudakis, A. Docoslis, *Polym. Degrad. Stabil.* **2008**, 93, 952.

11. M. Ganß, B. K. Satapathy, M. Thunga, R. Weidisch, P. P€otschke, D. Jehnichen, *Acta Mater*. **2008**, 56, 2247.

12. P. C. P. Watts, P. K. Fearon, W. K. Hsu, N. C. Billingham, H. W. Kroto, D. R. M. Walton, *J. Mater. Chem*. **2003**, 13, 491.

13. S. Morlat-Therias, E. Fanton, J.-L. Gardette, S. P. M. Alexandre, P. Dubois, *Polym. Degrad. Stabil*. **2007**, 92, 1873.

14. N. T. Dintcheva, F. P. L. V. Malatesta, *Polym. Degrad. Stabil.* **2009**, 94, 162.

15. L. Guadagno, C. Naddeo, M. Raimondo, G. Gorrasi, V. Vittoria, *Polym. Degrad. Stabil.* **2010**, 95, 1614.

16. A. L. Mart_ınez-Hern_andez, C. Velasco-Santos, V. M. Casta~no, *Curr. Nanosci.* **2010**, 6, 12.

17. J. Guo, Y. Liu, R. Prada-Silvy, Y. Tan, S. Azad, B. Krause, P. P€otschke, B. P. Grady, *J. Polym. Sci. Part B: Polym. Phys.* **2014**, 52, 73.

18. Y. Kato, D. J. Carlsson, D. M. Wiles, *J. Appl. Polym. Sci.* **1969**, 13, 1447.

19. D. J. Carlsson, D. M. Wiles, *Macromolecules* **1969**, 6, 597.

20. J. H. J Adams, *Polym. Sci.* Part A: *Polym. Chem.* **1970**, 8, 1077.

21. L. Audouin, V. Gueguen, A. Tcharkhtchi, J. Verdu, *J. Polym. Sci. Part A: Polym. Chem.* **1995**, 33, 921.

22. H. Nakatani, S. Suzuki, T. Tanaka, M. Terano, *Polymer* **2005**, 46, 12366.

23. W. Bauhofer, J. Z. Kovacs, *Compos. Sci. Technol.* **2009**, 69, 1486.

24. N. Sluzarenko, B. Heurtefeu, M. Maugey, C. Zakri, P. Poulin, S. Lecommandoux. *Carbon* **2006**, 44, 3207.

25. T. E. Chang, A. Kisliuk, S. M. Rhodes, W. J. Brittain, A. P. Sokolov, *Polymer* **2006**, 47, 7740.

26. P. P€otschke, T. Villmow, B. Krause, *Polymer* **2013**, 54, 3071.

27. H. Nakatani, S. Suzuki, T. Tanaka, M. Terano, *Polym. Int.* **2007**, 56, 1147.

28. K. Miyazaki, T. Arai, H. Nakatani, *J. Appl. Polym. Sci.* **2014**, 131, 39909.

29. J. S. Chong, E. B. Christiansen, A. D. Baer, *J. Appl. Polym. Sci.* **1971**, 15, 2007.

30. H. Nakatani, K. Miyazaki, *J. Appl. Polym. Sci.* **2013**, 129, 3490.

Achievement

Publication List

1. Hisayuki Nakatani, Keisuke Iwakura, Masato Hamadate, Noriyasu Okazaki, Masakazu Aoyama, Minoru Terano, “Interface Adhesion Properties of Syndiotactic Polypropylene/Cellulose Group Composite: Relationship Between Chemical Structure of Coupling Agent and Reactivity for Cellulose Group”, ***J. Appl. Polym. Sci.,*** **122**, 2798–2806, (2011).

2. Kensuke Miyazaki, Masato Hamadate, Minoru Terano, Hisayuki Nakatani, “Syndiotactic Polypropylene/Microfibrous Cellulose Composites: Effect of Filler Size on Tensile Properties”, ***J. Appl. Polym. Sci.,*** **128**, 915–922, (2013).

3. Masato Hamadate, Ryousaku Sato, Kensuke Miyazaki, Hisayuki Nakatani, “Additive Effects of Tripalmitin and Low-Density Polyethylene on Morphologies and Tensile Properties of Polybutene-1/micro Fibrous Cellulose Composite”, ***Polym. Bull.,*** **70** 3317-3330 (2013). IF＝1.44

4. Masato Hamadate, Ryousaku Sato, Kensuke Miyazaki, Noriyasu Okazaki, Hisayuki Nakatani, “Effect of Polymer Chain Scission on Photodegradation Behavior of Polystyrene/Multi-Wall Carbon Nanotube Composite”, ***J. Appl. Polym. Sci.***, **131**, 40362 (2014). IF=1.77

International Conference

[1] Masato Hamadate, Ryousaku Sato, Kensuke Miyazaki, Noriyasu Okazaki, Hisayuki Nakatani, “Degradation behavior of polystyrene/multiwall carbon nanotube composite” The 10th SPSJ International Polymer Conference, Tsukuba, Japan, 2014

Domestic Conference

[1] Masato Hamadate, Kensuke Miyazaki, Hisayuki Nakatani
“Syndiotactic polypropylene/ethanol swelled microfibrous cellulose composites: Development of a dispersion method and effect of filler size on tensile properties” The society of polymer science of Japan, Kanazawa, September, 2013

[2] Masato Hamadate, Ryousaku Sato, Kenesuke Miyazaki, Noriyasu Okazaki, Hisayuki Nakatani, “Effects of degradation of polystyrene / multi-walled carbon nanotube composites” The society of polymer science of Japan, Nagoya, May, 2014

[3] Masato Hamadate, Ryousaku Sato, Kensuke Miyazaki, Noriyasu Okazaki, Hisayuki Nakatani, “Effects of photodegradation on electrical conductivity of polystyrene/multiwall carbon nanotube composite” The 25th meeting of the materials life of Japan, Tokyo, July, 2014

[4]Masato Hamadate, Kensuke Miyazaki, Hisayuki Nakatani
“Syndiotactic polypropylene/ethanol swelled microfibrous cellulose composites: Development of a dispersion method and effect of filler size on tensile properties” The society of polymer science of Japan, Nagoya, September, 2014

Acknowlegement